ANL-7430
Engineering and Equipment
(TID-4500)
AEC Research and
Development Report

ARGONNE NATIONAL LABORATORY
9700 South Cass Avenue
Argonne, Illinois 60439

A STUDY OF ONE- AND TWO-COMPONENT, TWO-PHASE CRITICAL FLOWS AT LOW QUALITIES

by

Robert E. Henry

Reactor Engineering Division, ANL
and
Associated Midwest Universities

Based on a Thesis
Submitted to the Graduate School
of the University of Notre Dame
in Partial Fulfillment of the Requirements
for the Degree of
Doctor of Philosophy

March 1968

DISCLAIMER

TABLE OF CONTENTS

TABLE OF CONTENTS

LIST OF FIGURES

LIST OF FIGURES

LIST OF FIGURES

LIST OF TABLES

NOMENCLATURE

NOMENCLATURE

A	Cross-sectional area, ft^2
a	Velocity of sound, ft/sec
C_{efr}	Constant empty-to-full ratio
D	Diameter, ft
F	Frictional forces, lb_f/ft^2
f	Friction factor
G	Mass flow rate, $lb_m/sec\text{-}ft^2$
g_c	Gravitational constant, 32.17 $lb_m\text{-}ft/lb_f\text{-}sec^2$
H_0	Stagnation enthalpy, Btu/lb_m
h	Enthalpy, Btu/lb_m
I	Intensity of radiation, R/hr
I_0	Initial intensity of radiation, R/hr
J	Conversion factor, 778.2 $ft\text{-}lb_f/Btu$
k	Velocity ratio, u_g/u_ℓ
L	Length, ft
MM	Momentum multiplier, $lb_f\text{-}hr^2\text{-}in.^2/lb_m^2$
N	Experimental parameter
n	Polytropic exponent
P	Static pressure, lb_f/ft^2
s	Entropy, $Btu/lb_m\text{-}°F$
T	Temperature, °F
u	Velocity, ft/sec
v	Specific volume, ft^3/lb_m
x	Quality
y	Length, ft
Z	Axial length, ft

Greek Letters

α	Void fraction
γ	Isentropic exponent for a gas
Δ	Finite difference
θ	Head terms, lb_f/ft^2
μ	Attenuation coefficient, ft^{-1}
ρ	Density, lb_m/ft^3
ϕ_0	Empty signal, mV
ϕ_f	Full signal, mV
ϕ	Two-phase signal, mV

Subscripts

1,2	Arbitrary positions
c	Critical condition
E	Equilibrium
e	Exit plane
FZ	Frozen (dx/dP = 0)
f	Friction
fg	Difference between vapor and liquid quantities
g	Gaseous phase
H	Homogeneous (equal velocities)
ℓ	Liquid phase
M	Momentum
m	Mixture
R	Receiver
sat	Saturation
T	Total pressure loss
w	Wall

A STUDY OF ONE- AND TWO-COMPONENT, TWO-PHASE CRITICAL FLOWS AT LOW QUALITIES

by

Robert E. Henry

ABSTRACT

Two-phase, one-component critical flow was obtained in long tubes ($L/D > 40$) for mass flow rates of 512-6460 $lb_m/sec\text{-}ft^2$, exit pressures of 40-150 psia, and thermodynamic equilibrium qualities of 0.0019-0.216. Exit void fractions as well as axial void-fraction profiles were measured by a gamma-ray attenuation technique for void fractions of 0.07-0.94. These experimental void fractions resulted in velocity ratios that were considerably less than the existing analytical predictions.

The one-dimensional and steady-state approximations are experimentally justified for high-velocity flows with the aid of the measured axial void-fraction profiles.

Two test sections were designed to investigate the magnitude of two-dimensional effects at the exit plane. The two test sections were identical upstream of the exit plane. However, downstream of the exit, one test section diverged at a 7° included angle and the other at a 120° included angle. Results from these test sections indicate that previous experimental data are in considerable error for qualities below 10% because of the influence of the downstream two-dimensional expansion on the readings of wall-pressure taps located near the exit plane.

Although temperature and pressure were not measured simultaneously, the data exhibit trends that suggest the existence of a nonequilibrium phase change.

A model is developed to predict one-component, two-phase critical flow rates for equilibrium qualities less than 0.02. The model approximates the nonequilibrium processes of the real system by thermodynamic equilibrium paths and shows good agreement with the data for exit pressures of 50-150 psia. An analysis of the data and a comparison with the two-component data indicate that (1) the phase change occurring in the flow is of a nonequilibrium nature, and (2) the ratio of the average velocity of the two-phases is close to unity; that is, the flow is nearly homogeneous. Based on these indications, a homogeneous, partial-phase-change, sonic-velocity mechanism is proposed as an approximate explanation for the phenomenon of two-phase, one-component critical flow at low qualities.

CHAPTER I

INTRODUCTION

The existence of a maximum flow rate for which a fluid can pass through a converging nozzle or a constant-area duct at fixed stagnation conditions is well known from fluid-dynamic considerations of a compressible flow. In a single-phase flow, the critical discharge rate results in a sonic-velocity state at the throat of a converging nozzle or the exit plane of a constant-area duct. Such a system can also be composed of two separate phases which have greatly different bulk moduli, such as steam-water or air-water mixtures. The existence of a critical discharge rate for a two-phase system has been shown experimentally. However, the exact physical mechanism has not yet been demonstrated.[8,9,21]

The interest in two-phase critical flow evolved from its occurrence in cascade drain pipes of turbines and boilers as well as in the flow of refrigerants and condensing vapors. Further interest was generated by the safety aspects of water-cooled reactors. Critical flow determines the rate at which the radioactive coolant and contaminants are expelled from a ruptured reactor vessel or a primary piping system. The investigations initiated by these interests produced experimental data primarily in the quality range $0.01 \leq x_{Ee} \leq 1.0$.

The technology of liquid-sodium-cooled "fast reactors" and the associated safety problems also require a knowledge of the critical-flow phenomenon, but the physical characteristics of the system demand knowledge in a quality region where the validity of previous theoretical approaches is questionable. The formation of vapor (voidage) in a coolant channel may result in a positive reactivity coefficient for the reactor. Hence it is of vital importance to know how fast the voidage can be discharged, and the maximum discharge rate is determined by the critical-flow phenomenon. With a basic understanding of steam-water critical flow at low qualities, an extrapolation to sodium systems can be attempted. Even if a direct extrapolation cannot be performed, the results of the one-component, steam-water system will yield valuable information. The region of interest for these problems is a flow field that is better categorized by the void fraction ($0.0 < \alpha_e < 0.95$) than the quality.

The objectives of this research were:

1) To obtain one-component, two-phase, critical-flow data in the void-fraction range $0.20 < \alpha_e < 0.95$ and for exit pressures of 40-150 psia (which is the present range of interest in the fast-breeder reactor design).

2) To evaluate, on the basis of the experimental data, the validity of previous theoretical models in this range.

3) If the previous models were found to be incorrect, to develop a new model.

CHAPTER II

PREVIOUS WORK

A. Experimental Investigations

The following discussion will involve investigations that studied two-phase critical flow in long channels and will involve only works that appeared in the literature since 1957. A comprehensive literature survey of work before 1957 is given on pp. 11-20 of Ref. 9.

Isbin et al.[21] studied the critical flow of steam-water mixtures in various pipes and annuli for pressure and quality ranges of 4-43 psia and 0.01-1.0, respectively. They found that experimental mass flow rates were always greater than those predicted by the homogeneous equilibrium model. The authors presented an empirical correlation, based on their data, for the quality range of 0.01-1.0.

To accurately determine the exit-plane pressure, Faletti and Moulton[8] investigated steam-water critical flow in an annulus where the center rod served as a probe. The measured exit pressures were found to be lower than those obtained in Ref. 21 and this was attributed to a more precise throat-pressure measurement. The ratio G_c/G_{cHE} was found to be independent of the probe diameter and the exit pressures, for qualities greater than 0.15, and the test-section length, for lengths greater than 9 in. For the quality range of 0.02-0.15, the ratio G_c/G_{cHE} was depressed with increasing throat pressure. The addition of surface agents (detergent) to reduce the surface tension increased the exit pressure but did not affect the mass flow rate. A correlation for G_c/G_{cHE} in the quality range of 0.25-0.95 was presented.

Zaloudek[49] conducted an experimental investigation that was similar to that of Faletti and Moulton except that his test sections had circular full-bore cross sections, and his exit pressure was evaluated from a wall tap located slightly upstream of the exit plane. His results, for qualities greater than 0.20, and the correlation presented for this range are nearly identical to those given in Ref. 8. The only difference between Zaloudek's observations and those of Faletti and Moulton occurs in the pressure dependency of the G_c/G_{cHE} ratio for qualities of 0.02-0.20. Both investigations witnessed the dependency; however, the magnitude of the variation differs.

Fauske[9] obtained steam-water critical-flow data for high exit pressures (40 psia $\leq P_e \leq$ 360 psia) and qualities ($0.01 \leq x_{Ee} \leq 0.70$). This was the first high-pressure experimentation performed. The theoretical model developed in Ref. 9 will be discussed in Part B of this chapter.

In 1963, Cruver[4] presented a dissertation on the phenomenon of metastability in one-component, two-phase critical flow. The existence of metastability was determined by simultaneous temperature and pressure measurements. Superheats (up to 14°F) and supercooling (up to 7.5°F) were measured when the expansion produced net evaporation or net condensation, respectively. The overall critical-flow data obtained by Cruver compared favorably with that of Refs. 8 and 49. Cruver developed a separated-flow model, which is discussed in Part B of this chapter.

Klingebiel[29] determined the ratio of average vapor to liquid velocities in steam-water critical flow by measuring the thrust of the expanding free jet with a modified impulse plate. The velocity ratios at the exit plane decreased from 5.05 to 1.34 with increasing quality, which is not the behavior predicted by separated-flow models. Klingebiel attributed the discrepancies between the measured and predicted velocity ratios to entrainment of the liquid in the vapor phase. He also investigated the pressure distribution near the exit plane by comparing pressure measurements recorded by means of a centerline probe with those determined by wall-pressure taps located within 0.005 in. of the exit plane. Discrepancies between the two measurements indicated that the static pressure varied radially near the throat, and this variation was ascribed to a wall effect.

In a paper presented at the University of Exeter, Fauske[14] reported exit velocity ratios in air-water critical flow. The velocity ratios, which were determined by measuring the exit void fractions using a gamma-ray attenuation technique, ranged from 1.13 to 2.39 and increased with increasing quality. Visual observation of the flow regime at the exit plane revealed either bubbly or highly dispersed distributions rather than separated phases as assumed by the theoretical models. Fauske concluded that the good agreement between theoretical models and experimental data was a result of high velocity ratios compensating for the presence of metastability in the flow.

In 1966, Uchida and Nariai[46] studied the discharge of saturated water through pipes and orifices. The flow was observed by means of a high-speed camera, which showed that the actual flow regime is one of a froth or mist flow.

B. Theoretical Models Proposed

Fauske[9] developed a critical-flow model based on the proposed criterion that at critical-flow conditions the magnitude of the pressure gradient at the exit is a maximum for a given quality and flow rate.

The model assumed that the expansion occurred in an equilibrium manner and that the phase-change term could be expressed as an isenthalpic process. These assumptions and the above criterion caused a minimization

of the momentum specific volume, which resulted when $k = \sqrt{v_g/v_\ell}$. This approach exhibited good agreement with the overall experimental data (pressure, flow rate, and equilibrium quality) in a quality range ($0.01 \leq x_{Ee} \leq 1.0$). However, the predicted velocity ratios are much greater than those observed in Refs. 14 and 29.

Moody[35] derived a critical-flow equation from the energy equation and used the assumptions of equilibrium and constant entropy. The result of this approach was a minimization of the energy specific volume, which occurred when $k = \sqrt[3]{v_g/v_\ell}$. This was essentially the result obtained by Zivi,[52] who used the principle of minimum entropy production in a steady-state process. This principle states that minimum entropy production is achieved when the kinetic energy is a minimum. Thus, for a given flow rate, the kinetic energy will minimize when the energy specific volume reaches its minimum ($k = \sqrt[3]{v_g/v_\ell}$). The model developed by Moody displays good agreement with the data for equilibrium qualities between 0.01 and 1.0. However, the predicted velocity ratios are much greater than those observed experimentally. For a constant critical exit pressure, this model predicts increasing flow rates for decreasing qualities until the quality becomes less than 0.01, where the flow rates decrease with quality.

Cruver[4] also developed a model that resulted in the prediction that $k = \sqrt[3]{v_g/v_\ell}$. He showed there are three mixture specific volumes: the energy specific volume, which minimizes when $k = \sqrt[3]{v_g/v_\ell}$; the momentum specific volume, which minimizes when $k = \sqrt{v_g/v_\ell}$; and the continuity specific volume, which never minimizes with respect to the velocity ratio. Cruver reasoned that since the energy specific volume minimized at the lowest value of the velocity ratio, a higher value would increase the total energy requirement of the flow. Hence the velocity ratio of $k = \sqrt[3]{v_g/v_\ell}$ is the maximum value that may exist in two-phase separated flow.

In 1965, Levy[31] presented a theoretical approach which assumed that all frictional losses (including interfacial shear) and head losses were negligible. This assumption allowed him to subtract the momentum equations for each phase and thereby obtain another equation relating the quality and void fraction. He also assumed an isentropic equilibrium expansion. This approach produced results in the quality range 0.01-1.0, that were almost identical with the theoretical predictions of Ref. 9. It also exhibits a maximum in a plot of flow rate versus quality, as was described above in the discussion of Moody's theoretical model.

CHAPTER III

ANALYSIS

A. The Critical-flow Criterion

The one-dimensional explanation of a critical discharge for adiabatic single-phase flow is well defined, both physically and mathematically. Physically, the flow is choked at the throat of a converging nozzle or a constant-area duct when the fluid is accelerated to the sonic velocity associated with the throat temperature. Since the fluid velocity is equal to the propagation velocity of a pressure wave, the receiver pressure cannot propagate into the duct to accelerate the flow to a greater velocity. Hence the flow is choked. The inability of the receiver pressure to propagate into the duct renders the flow rate independent of variations in P_R. For subsonic flows in the above geometrices, one assumes that $P_R = P_e$. Hence, mathematically the exit pressure is decreased until this maximum flow rate is obtained. This condition may be expressed as

$$\left(\frac{\partial G_c}{\partial P_e}\right)_s = 0.$$

The designation of constant entropy is a result of approximations to the one-dimensional momentum equation,

$$u\frac{du}{dZ} = -v\frac{dP}{dZ} - v\frac{dF_w}{dZ} - v\frac{d\theta}{dZ}. \tag{3-1}$$

Near the exit plane of a constant-area duct or a converging nozzle, the pressure decrease due to the increase in momentum is assumed to be much larger than the losses due to friction and head drop. Therefore Eq. 3-1 results in the approximate momentum equation

$$u_e\left(\frac{\partial u_e}{\partial Z}\right)_s = -v_e\left(\frac{\partial P_e}{\partial Z}\right)_s. \tag{3-2}$$

The isentropic designation is assigned because the assumption of no wall friction makes the momentum equation reversible; for adiabatic flow, this assumption implies an isentropic expansion.

A general expression for the critical discharge rate can be obtained by using the continuity and momentum equations. Differentiating the continuity equation ($Gv = u$) and applying the critical-flow criterion gives

$$\left(\frac{\partial u_e}{\partial P_e}\right)_s = G_c\left(\frac{\partial v_e}{\partial P_e}\right)_s. \tag{3-3}$$

Substitution of Eq. 3-3 into Eq. 3-2 produces

$$G_c^2 = -g_c\left(\frac{\partial P_e}{\partial v_e}\right)_s .$$

Note that this relationship can be obtained for flow in an adiabatic, frictionless, constant-area duct without using the critical-flow criterion. This result implies that the only nonzero velocity that may exist throughout the duct under these ideal conditions is the sonic velocity. The above expression for G_c^2 is the relationship for the maximum mass flow rate of a single-phase fluid at a given exit pressure and temperature. Since the flow is isentropic, the pressure and volume follow the polytropic process $Pv^\gamma = C$ where C is a constant. Therefore

$$G_c^2 = \frac{g_c \gamma P_e}{v_e}, \tag{3-4}$$

and the velocity at the throat must equal

$$u_e^2 = g_c \gamma P_e v_e = a^2, \tag{3-5}$$

which indeed shows the throat velocity to be equal to the speed of pressure-wave propagation.

The same approach was initially attempted for two-phase critical flow. Physical reasoning dictated that isentropic adiabatic flow in a two-phase media would be a thermodynamic equilibrium process, which implies that the two phases have the same velocity and temperature. (For a one-component system, the temperature of the fluid also corresponds to the saturation temperature for a given system pressure.) This resulted in the homogeneous equilibrium model. (The term homogeneous implies equal velocities for the phases.) The development is identical to that of Eqs. 3-1 through 3-3 except that the specific volume is defined as

$$v = (1 - x_E)\, v_\ell + x_E v_g .$$

With this definition of the specific volume, the critical-flow equation for homogeneous equilibrium flow may be written as

$$G_{cHE}^2 = -g_c\left(\frac{\partial P_e}{\partial v_e}\right)_s = \frac{-g_c}{\left\{x_E\left(\frac{\partial v_g}{\partial P}\right)_s + (v_g - v_\ell)\left(\frac{\partial x_E}{\partial P}\right)_s + (1 - x_E)\left(\frac{\partial v_\ell}{\partial P}\right)_s\right\}_e},$$

where the subscript e requires that the system variables and their derivatives be evaluated at the exit plane. (This notation will be used throughout this report.)

At moderate pressures ($P_e < 200$ psia), the relative magnitudes of the specific volume and compressibility of water with respect to those of steam are

$$v_\ell / v_g < 10^{-2}$$

and

$$\frac{\left(\frac{\partial v_\ell}{\partial P}\right)_s}{\left(\frac{\partial v_g}{\partial P}\right)_s} < 10^{-3}.$$

Thus, the homogeneous equilibrium critical flow equation may be approximated as

$$G^2_{cHE} = \frac{-g_c}{\left\{x_E\left(\frac{\partial v_g}{\partial P}\right)_s + v_g\left(\frac{\partial x_E}{\partial P}\right)_s\right\}_e}.$$

When $x_E < 10^{-3}$, so that $x_E(\partial v_g/\partial P)_s$ and $(1 - x_E)(\partial v_\ell/\partial P)_s$ are of the same magnitude, $v_g(\partial x_E/\partial P)$ is the only sizable term in the equation. Hence any error induced by this approximation is insignificant. When $x_E = 1.0$ and $(\partial x_E/\partial P)_s = 0$, which is the single-phase case, the above relation reduces to the single-phase critical-flow equation.

Many investigators[8,9,21,49] have shown that the flow rates predicted by the homogeneous equilibrium model are considerably less than those obtained experimentally. Two reasons are usually cited to explain why the experimental flow rates are higher:

1. The density difference between the phases allows greater acceleration of the gas than the liquid for the same pressure decrease. Consequently, the velocities of each phase may differ significantly. The fact that the ratio of the phase velocities $k = u_g/u_\ell$ (velocity ratio) is different from unity has been shown to be one reason for a discrepancy between the homogeneous equilibrium model and experimental data.[14]

2. Critical flow is characterized by large pressure gradients near the exit plane. In this region, the system pressure may decrease so rapidly that the phase change cannot follow an equilibrium process. At qualities less than approximately 50%, where expansion produces net evaporation, a lag in the phase change would cause both the actual quality and the rate of phase change to be less than their thermodynamic equilibrium values. These two phenomena would decrease the compressibility of the system and thus result in a flow rate greater than the equilibrium case.

For flow in long ducts, the first reason above has received more attention than the second reason. Several thermodynamic equilibrium models,[9,31,35] which incorporate the velocity ratio, were discussed in Chapter II. These models show good agreement at qualities of 0.01-1.00. However, all the models predict velocity ratios that are much higher than those witnessed at and near critical flow.[14,29,47] Consequently, these models are useful correlations, but they do not appear to correctly outline the actual variation of the physical parameters.

The second reason mentioned has received little attention. The attempt to account for nonequilibrium in the low-quality region has been one of assuming "frozen flow" ($dx/dP = 0$) at the exit plane, i.e., no phase change at the throat.[14,41] This assumption has been used in conjunction with various correlations for the velocity ratio.[6] However, the relationship between this approximation and the physical process is questionable because the "frozen-flow" assumption is used with the thermodynamic equilibrium quality. This type of approach assumes that the fluid expands in an equilibrium manner to the exit plane and then passes through the exit in a frozen state. A more logical situation would involve the presence of a nonequilibrium state before, as well as at, the exit, and as the fluid passes through the exit plane, a phase change occurs. In this state, the actual quality would not be equal to the thermodynamic equilibrium quality and dx/dP would not equal zero.

To begin the theoretical study of two-phase critical flow, the criterion can be determined in light of experimental evidence. As was shown earlier in this chapter, single-phase choked flow can be related to the speed of a pressure-wave propagation. Such a concise relationship is not easily determined in a two-phase mixture. However, several experimental investigators[8,21,29,49] have witnessed that the flow rate reaches a maximum with respect to the receiver pressure and that a further reduction in this pressure fails to change the flow. From this experimental information, one can mathematically express the phenomenon as $(\partial G_c/\partial P_e)_{path} = 0$, since P_e and P_R are theoretically the same until the critical condition is obtained. The path restriction on the partial derivative, however, cannot be immediately specified as isentropic. To determine the nature of the path, one must examine the equations governing the behavior of a two-phase fluid.

The one-dimensional, steady-flow equations for adiabatic two-phase flow in a constant area duct are given below.[9,29,31]

1. Continuity

For the vapor phase,

$$\frac{d}{dZ}\left(\frac{A_g u_g}{v_g x}\right) = 0. \qquad (3\text{-}6)$$

For the liquid phase,

$$\frac{d}{dZ}\left[\frac{A_\ell u_\ell}{v_\ell (1-x)}\right] = 0. \tag{3-7}$$

2. Momentum

$$-\frac{dP}{dZ} = \frac{G}{g_c}\frac{d}{dZ}\left[xu_g + (1-x)\,u_\ell\right] + \frac{dF_w}{dZ} + \frac{d\theta}{dZ}. \tag{3-8}$$

3. Energy

$$\frac{d}{dZ}\left[(1-x)\,h_f + xh_g\right] = -\frac{1}{2g_c J}\frac{d}{dZ}\left[xu_g^2 + (1-x)\,u_\ell^2\right]. \tag{3-9}$$

It was pointed out previously that an isentropic adiabatic expansion in two-phase flow must be in thermodynamic equilibrium. Hence each phase must have the same velocity and temperature. This condition, unfortunately, does not exist if nonequilibrium states and velocity differences are present. These irreversible processes in the free stream directly affect the momentum equation because the central core of the fluid is not isentropic. This result suggests that the criterion set forth in a single-phase flow is not sufficient for two-phase flow.

Examination of the governing equations for two-phase flow reveals that the only one system property to be constant is the stagnation enthalpy. This property is constant for any adiabatic flow. Therefore the most general criterion for critical flow is

$$\left(\frac{\partial G_c}{\partial P_e}\right)_{H_0} = 0. \tag{3-10}$$

This criterion must hold for single- or two-phase Fanno flow. If the flow is approximately isentropic, as in the single-phase case, then

$$\left(\frac{\partial G_c}{\partial P_e}\right)_s = \left(\frac{\partial G_c}{\partial P_e}\right)_{H_0} = 0.$$

B. General Equation for Critical Flow

Based on the general criterion discussed above, one can derive a critical-flow relationship that is valid for single- or two-phase flow.

Assume that, like the single-phase case, the momentum pressure drop near the exit plane is much larger than the sum of the frictional and

head losses. This approximation, plus the restriction of constant stagnation enthalpy, reduces the momentum equation to

$$-\left(\frac{\partial P_e}{\partial Z}\right)_{H_0} = \frac{G}{g_c}\frac{\partial}{\partial Z}\left[\left\{x u_g + (1-x)\, u_\ell\right\}_e\right]_{H_0}$$

or

$$-1 = \frac{G}{g_c}\frac{\partial}{\partial P_e}\left[\left\{[xk + (1-x)]\, u_\ell\right\}_e\right]_{H_0}. \tag{3-11}$$

Integration of the continuity equations leads to the following expressions:

For the vapor phase,

$$xG = \frac{\alpha u_g}{v_g};$$

for the liquid phase,

$$(1-x)\, G = \frac{(1-\alpha)\, u_\ell}{v_\ell};$$

where

$$\alpha = A_g/A \text{ and } 1 - \alpha = A_\ell/A.$$

These two independent relations may be rearranged into the following more convenient forms:

$$G = \left[\frac{\alpha k}{v_g} + \frac{1-\alpha}{v_\ell}\right] u_\ell \tag{3-12}$$

and

$$\alpha = \frac{x v_g}{k(1-x)\, v_\ell + x v_g}. \tag{3-13}$$

Equation 3-13 may be substituted into Eq. 3-12 and simplified to

$$G = \left[\frac{k}{k(1-x)\, v_\ell + x v_g}\right] u_\ell. \tag{3-14}$$

Substituting the continuity equation, Eq. 3-14, into the momentum equation gives

$$-1 = \frac{G}{g_c}\frac{\partial}{\partial P_e}\left[\left\{\frac{G[k(1-x)\,v_\ell + xv_g][xk + (1-x)]}{k}\right\}_e\right]_{H_0}.$$

The critical-flow criterion states

$$\left(\frac{\partial G_c}{\partial P_e}\right)_{H_0} = 0.$$

Therefore,

$$G_c^2 = \frac{-g_c}{\dfrac{\partial}{\partial P_e}\left[\left\{\dfrac{[k(1-x)\,v_\ell + xv_g]\,[xk + (1-x)]}{k}\right\}_e\right]_{H_0}}. \tag{3-15}$$

This is the general expression for single- or two-phase critical flow. If the expression is expanded, several order-of-magnitude approximations can be made. Differentiation of Eq. 3-15 results in

$$\begin{aligned} G_c^2 = -g_c\Bigg\{ & k\Bigg[\{[1 + x(k-1)]\,x\}\left(\frac{\partial v_g}{\partial P}\right)_{H_0} \\ & + \{v_g[1 + 2x(k-1)] + kv_\ell[2(x-1) + k(1-2x)]\}\left(\frac{\partial x}{\partial P}\right)_{H_0} \\ & + \{k[1 + x(k-2) - x^2(k-1)]\}\left(\frac{\partial v_\ell}{\partial P}\right)_{H_0} \\ & + x(1-x)\left(kv_\ell - \frac{v_g}{k}\right)\left(\frac{\partial k}{\partial P}\right)_{H_0}\Bigg]^{-1}\Bigg\}_e. \end{aligned} \tag{3-16}$$

Two investigators[14,29] have experimentally determined the velocity ratios for critical flow at low pressures (15 psia $< P_e <$ 40 psia), and their results show the magnitude to be of the order of 2 or 3, not 20 or 30. The velocity ratio is mainly a result of the density difference between the phases. Therefore, at higher pressures ($P_e \geq$ 50 psia), the velocity ratio should be even smaller because the density difference is reduced.

Using the order-of-magnitude approximations listed on p. 18 and the experimental fact that the velocity ratio is

$$k \sim 0(1) \ll \sqrt{\frac{v_g}{v_\ell}} \sim 0(10),$$

one can simplify Eq. 3-16 to

$$G_c^2 = -g_c \left\{ k \left[[1 + x(k-1)] \, x \left(\frac{\partial v_g}{\partial P} \right)_{H_0} + v_g [1 + 2x(k-1)] \left(\frac{\partial x}{\partial P} \right)_{H_0} \right. \right.$$
$$\left. \left. - x(1-x) \frac{v_g}{k} \left(\frac{\partial k}{\partial P} \right)_{H_0} \right]^{-1} \right\}_e . \qquad (3\text{-}17)$$

Equation 3-17 can be applied to single-phase critical flows, which by definition require that $(\partial x/\partial P)_{H_0} = 0$, and that either $x = 0$ or $x = 1$, depending on whether the phase is liquid or gaseous. For gaseous flow ($x = 1$), Eq. 3-17 reduces to

$$G_c^2 = -g_c \left(\frac{\partial P_e}{\partial v_{ge}} \right)_{H_0},$$

which is the same as the single-phase equation derived earlier in this chapter. (The equivalence of isentropic and constant stagnation-enthalpy paths for single-phase flow was discussed previously in this chapter.) For liquid flow ($x = 0$), Eq. 3-17 results in an infinite flow rate, which is a consequence of the order-of-magnitude assumption that presumes the liquid is incompressible.

C. An Approximation for Critical Flow at Low Qualities

The partial derivatives in Eq. 3-17 are all characteristic of a non-equilibrium process due to the nature of the flow. Since the only derivatives one can evaluate are those of an equilibrium process, Eq. 3-17 could be solved if it could be related to an equilibrium process.

Assume

$$x = kNx_E, \qquad (3\text{-}18)$$

so that

$$\left(\frac{\partial x}{\partial P} \right)_{H_0} = kN \left(\frac{\partial x_E}{\partial P} \right)_{H_0} + kx_E \left(\frac{\partial N}{\partial P} \right)_{H_0} + Nx_E \left(\frac{\partial k}{\partial P} \right)_{H_0}, \qquad (3\text{-}19)$$

where N is a characteristic parameter of the system. When $x < 0.50$, the net process in a decreasing-pressure field is one of evaporation. This implies that any lag in the phase change will cause the actual quality to be less than the thermodynamic equilibrium value ($x \leq x_E$) In the large negative pressure gradients associated with critical flow, the average velocity of the gas should be greater than that of the liquid ($k > 1.0$). These two facts require that (1) $kN \leq 1.0$ and (2) $N < 1.0$.

Substitution of Eqs. 3-18 and 3-19 into Eq. 3-17 produces

$$G_c^2 = -g_c \Bigg[k \Bigg\{ [1 + kNx_E(k-1)]\, kNx_E \left(\frac{\partial v_g}{\partial P}\right)_{H_0} + v_g [1 + 2kNx_E(k-1)] \left[kN \left(\frac{\partial x_E}{\partial P}\right)_{H_0} + Nx_E \left(\frac{\partial k}{\partial P}\right)_{H_0} + kx_E \left(\frac{\partial N}{\partial P}\right)_{H_0} \right] - Nx_E(1 - kNx_E)\, v_g \left(\frac{\partial k}{\partial P}\right)_{H_0} \Bigg\}^{-1} \Bigg]_e , \tag{3-20}$$

If $x_{E_e} < 0.02$, then $(kNx_E)_e < 0.02$, and if k_e is no more than 2 or 3, several quantities are small with respect to unity. (It will be argued in Chapter V that, for one-component mixtures in this quality range, the velocity ratio is very close to 1.0.) This approximation for low qualities ($x_{E_e} < 0.02$) simplifies Eq. 3-20 to

$$G_c^2 = \frac{-g_c}{\left\{ Nx_E \left(\frac{\partial v_g}{\partial P}\right)_{H_0} + v_g N \left(\frac{\partial x_E}{\partial P}\right)_{H_0} + v_g x_E \left(\frac{\partial N}{\partial P}\right)_{H_0} \right\}_e} , \tag{3-21}$$

where $(\partial x_E/\partial P)_{H_0}$ is the derivative of a thermodynamic equilibrium quantity. Hence, since it is an equilibrium parameter, it is associated with the reversible behavior of the adiabatic system. The adiabatic and reversible restrictions require that the process be isentropic. When a process is isentropic and adiabatic, constant entropy and constant stagnation enthalpy are identical paths; this was also discussed in Part A of this chapter. This results in

$$\left(\frac{\partial x_E}{\partial P_e}\right)_{H_0} = \left(\frac{\partial x_E}{\partial P_e}\right)_s ,$$

where $(\partial x_E/\partial P_e)_s$ may be evaluated from the steam tables.[27]

The derivative $(\partial v_g/\partial P_e)_{H_0}$ is determined by the real system and thus is not an equilibrium derivative. However, the vapor expansion can be represented as a polytropic process, and since heat is being transferred to the vapor and its temperature is still decreasing, the polytropic exponent must lie between $1.0 < n < 1.3$. It is difficult to determine the value of n, but for $x_E = 0.01$ the term $x_E(\partial v_g/\partial P_e)_{H_0}$ is 10% of $v_g(\partial x_E/\partial P_e)_{H_0}$. The variation of n affects the final calculation of the critical flow rate by only 1%. Thus it makes little difference what value is assumed for the exponent n. To facilitate calculations, the polytropic exponent will be assumed to be unity.

Equation 3-21 can now be written as

$$G_c^2 = \frac{g_c}{\left\{N\left[\frac{x_E v_g}{P} - v_g\left(\frac{\partial x_E}{\partial P}\right)_s\right] - v_g x_E\left(\frac{\partial N}{\partial P}\right)_{H_0}\right\}_e}. \tag{3-22}$$

Equation 3-22 shows that the critical-flow expression for low qualities has been related to thermodynamic equilibrium paths with respect to the vapor expansion and the phase change. Comparing this equation with Eq. 3-17 shows that only the variable N and its derivative remain as unknowns, whereas, previously one had to evaluate x, k, and their derivatives. All the irreversibilities involved in the real process, such as slip between the phases and retardation of the phase change, are encompassed by the terms N_e and $(\partial N_e/\partial P_e)_{H_0}$.

At low qualities $[(1 - x) \approx 1]$, Eq. 3-13 may be approximated as

$$x = k\frac{\alpha}{1 - \alpha}\frac{v_\ell}{v_g}. \tag{3-23}$$

Comparing Eqs. 3-23 and 3-18 shows that

$$N = \frac{\alpha v_\ell}{x_E(1 - \alpha)\, v_g}. \tag{3-24}$$

The parameter N is a combination of parameters which have been determined experimentally in this study. As was noted previously, N is a measure of the difference between the real and isentropic processes at the point of choking. (Wall friction was neglected in both developments.) If no irreversibilities are present, N_e would equal unity and $(\partial N_e/\partial P_e)_{H_0} = 0$. Figure 1 shows experimental values of N_e, which is clearly less than unity, as the result of the irreversible processes of slip between the phases and the nonequilibrium nature of the phase change.

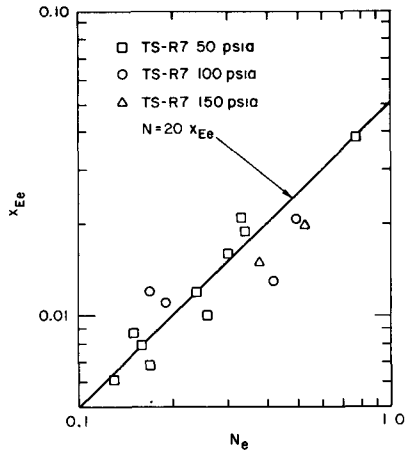

112-9287

Fig. 1. Experimental Values of N_e

To be useful in predicting critical flow rates, N must be correlated with respect to an equilibrium quantity since the equilibrium parameters can be evaluated without witnessing the actual flow. Figure 1 illustrates the relationship between N_e and x_{Ee} for three different exit pressures. The variations in the data can result from inaccuracies in the void-fraction measurement or from a pressure dependency in the relationship between x_{Ee} and N_e. As a first approximation, assume that N_e is only a function of x_{Ee}. The data points of Fig. 1 were correlated with a linear least-squares technique, which resulted in the function plotted in the figure.

To investigate the term $(\partial N_e/\partial P_e)_{H_0}$, one must know axial profiles of void fraction and pressure. The void-fraction profiles were measured by traversing the duct with the gamma-ray equipment from position U5 upstream of the throat and proceeding through the exit plane. Figure 2 displays the variations of P and N as functions of Z near the exit plane for three experimental runs of Test Section R7.* The derivative $(\partial N_e/\partial P_e)_{H_0}$ may be expressed as the quotient $(\partial N/\partial Z)_{H_0}/(\partial P/\partial Z)_{H_0}$ evaluated at the exit plane. As illustrated by the graphs in Fig. 2, $(\Delta P/\Delta Z)_{H_0}$ is large very near the throat, but $(\Delta N/\Delta Z)_{H_0}$ is relatively small. Therefore, as a first approximation, $(\partial N_e/\partial P_e)_{H_0}$ may be assumed to be zero. The validity of this approximation will be discussed in Chapter V. (Note that in the lower illustration of Fig. 2, the value of N at position U5 is greater than unity, and in fact is infinite at this point. This apparent contradiction will be discussed in Section E of Chapter V, and arguments will be presented to show that this behavior is not unexpected.) The assumption that $(\partial N_e/\partial P_e)_{H_0} = 0$ reduces Eq. 3-22 to

$$G_c^2 = \frac{g_c}{\left\{ N \left[\frac{x_E v_g}{P} + v_g \left(\frac{\partial x_E}{\partial P} \right)_s \right] \right\}_e} \qquad (3\text{-}25)$$

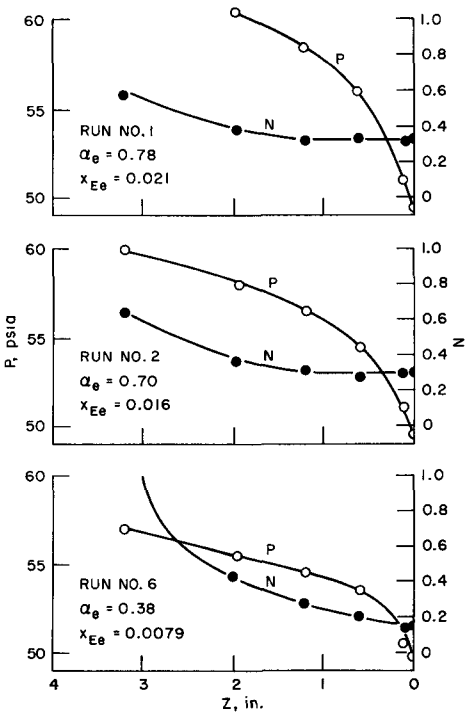

112-9292

Fig. 2. Experimentally Determined Axial Variations of N and P in the Vicinity of the Exit Plane

*The test sections used in this study are identified as R7, C7, and C120, where R and C refer to rectangular and circular cross-sectional areas of flow, respectively, and the numbers 7 and 120 refer to the number of degrees in the included angle of divergence of the expansion chamber. In some of the figures in this report, for the convenience of the reader, the test sections are labeled TS-R7, TS-C7, and TS-C120.

or simply

$$\frac{G_c}{G_{cHE}} = \sqrt{\frac{1}{N_e}}. \tag{3-26}$$

The above model used experimental data for one-component, two-phase critical flows to evaluate the parameter N, and hence is only valid for such flows. It was shown that N simplified the treatment of the partial derivatives representing the rates of change of the phases and the velocity ratio. It is interesting to pursue a similar derivation for two-component, two-phase critical flows at low qualities.

In two-component flow there is no phase change, and thus $(\partial x/\partial P)_{H_0} = 0$. This condition reduces the previously derived homogeneous equilibrium critical-flow equation to

$$G_{cH}^2 = \frac{-g_c}{\left[x\left(\frac{\partial v_g}{\partial P}\right)_{H_0} + (1-x)\left(\frac{\partial v_\ell}{P}\right)_{H_0}\right]_e}.$$

The E subscript is dropped from the quality because it is meaningless to speak of an equilibrium or a nonequilibrium quality in a flow where there is no change of phase. The equilibrium notation is also dropped from the flow rate to avoid confusion with the homogeneous equilibrium equation for one-component flows. Since irreversibilities may arise due to a temperature difference between the phases, the equilibrium restriction would require that the phases exist at the same temperature. In the adiabatic expansion of air and water, the water loses heat to the air. For low-quality flows ($x < 0.02$), the mass of the liquid is so much larger than that of the air, that an equilibrium expansion is approximately the same as an isothermal one. As has been discussed elsewhere,[36] the heat-transfer rates between the phases also appear to justify an isothermal approximation for the real path of the fluid. Since there seems to be little discrepancy between equilibrium and real processes with respect to temperature differences between the phases, the equilibrium notation is not used in conjunction with two-component flow.

For low-quality flows, the equilibrium path may be approximated by the isothermal path. Thus the two-component homogeneous critical-flow equation may be written as

$$G_{cH}^2 = \frac{-g_c}{\left[x\left(\frac{\partial v_g}{\partial P}\right)_T + (1-x)\left(\frac{\partial v_\ell}{\partial P}\right)_T\right]_e}.$$

If the air is assumed to be a perfect gas, the relative magnitude of the isothermal compressibility of the water to that of air for pressures near atmospheric is

$$\frac{\left(\frac{\partial v_\ell}{\partial P}\right)_T}{\left(\frac{\partial v_g}{\partial P}\right)_T} \approx 10^{-7}.$$

Thus the compressibility of the water may be neglected for $x > 10^{-5}$. This approximation allows one to express the homogeneous critical flow rate for two-component, two-phase flows as

$$G_{cH}^2 = \frac{g_c}{\left(\frac{x v_g}{P}\right)_e}.$$

The general equation of two-phase critical flow of two-component fluids may be obtained by applying the $(\partial x/\partial P)_{H_0} = 0$ criterion to Eq. 3-16. (The same order-of-magnitude approximations apply here.) The result is

$$G_c^2 = -g_c \left\{ k \left[[1 + x(k-1)] \, x \left(\frac{\partial v_g}{\partial P}\right)_{H_0} - x(1-x) \frac{v_g}{k} \left(\frac{\partial k}{\partial P}\right)_{H_0} \right]^{-1} \right\}_e . \qquad (3\text{-}27)$$

For low qualities ($x_e < 0.02$), this relation may be further simplified to

$$G_c^2 = -g_c \left\{ k \left[x \left(\frac{\partial v_g}{\partial P}\right)_T - x \frac{v_g}{k} \left(\frac{\partial k}{\partial P}\right)_T \right]^{-1} \right\}_e \qquad (3\text{-}28)$$

The form of Eq. 3-28 resembles that of Eq. 3-22 in that the only remaining unknowns are k_e and $(\partial k_e/\partial P_e)_{H_0}$, whereas previously they were N_e and $(\partial N_e/\partial P_e)_{H_0}$. It is not unexpected that there is a similarity between k and N in the two-component case as illustrated by Eq. 3-18 when $x = x_E$ (two-component flow). In this case, the relation between N and k is

$$N = 1/k.$$

In the discussion of one-component flow, it was stated that N is a measure of the irreversibilities of the system, which are slip between the phases and retardation of the phase change. In two-component flows, there is no phase change. Hence the only apparent irreversibility is a velocity difference between the liquid and the gas. The effect of this nonequilibrium state is measured by k and its derivative. Therefore the quantity N is of no aid in two-component flow.

Experimental values of the exit-plane velocity ratio for two-component, two-phase critical flows have been reported in Ref. 14. The evaluation of the quantity $(\partial k_e/\partial P_e)_{H_0}$, which may be written as $\left[(\partial k/\partial Z)_{H_0}/(\partial P/\partial Z)_{H_0}\right]_e$, requires axial void-fraction profiles like those used in determining $(\partial N_e/\partial P_e)_{H_0}$. This information has not yet been published in the literature, but one might expect $(\partial k_e/\partial P_e)_{H_0}$ to become small, either in the low void-fraction region ($\alpha_e < 0.20$), where widely separated bubbles are entrained in the liquid, or at elevated pressures where the density ratio is small. The assumption of $(\partial N_e/\partial P_e)_{H_0} = 0$ for one-component flow does not infer in any way that $(\partial k_e/\partial P_e)_{H_0} = 0$ for two-component flow. Differentiating Eq. 3-18 and setting $(\partial N_e/\partial P_e)_{H_0} = 0$ reveals that for such a condition to exist, the following relation must hold:

$$\left(\frac{\partial x_e}{\partial P_e}\right)_{H_0} = \left\{ x\left[\frac{1}{k}\left(\frac{\partial k}{\partial P}\right)_{H_0} + \frac{1}{x_E}\left(\frac{\partial x_E}{\partial P}\right)_{H_0}\right]\right\}_e .$$

An interplay between the change of phase and the velocity-ratio derivatives could result in $(\partial N_e/\partial P_e)_{H_0} = 0$. Such an interplay is not possible in two-component flow. The assumption that $(\partial k_e/\partial P_e)_{H_0} = 0$ should produce an asymtotic solution which becomes more exact at small void fractions or elevated pressures. This simplifies Eq. 3-28 to

$$G_c^2 = \left(\frac{-g_c k P}{x v_g}\right)_e \tag{3-29}$$

or

$$\frac{G_c}{G_{cH}} = \sqrt{k_e}. \tag{3-30}$$

The above relations for one- and two-component, two-phase critical flows along with previous theoretical models are compared with experimental data in Chapter V.

CHAPTER IV

EXPERIMENTAL INVESTIGATION

The experimental critical-flow data were obtained with the instrumented test section extending from the blow-down vessel as shown in the schematic diagram of the experimental apparatus (Fig. 3). The operating proceedure, test section, and major component, as well as basic measurement techniques, are described in this chapter. The resulting experimental data are summarized in tabular form in Appendix D.

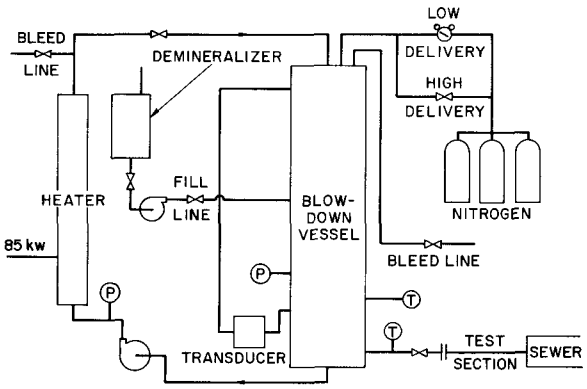

112-9310

Fig. 3. Experimental Apparatus, Schematic Diagram

A. Operating Procedure

The operating procedure is as follows:

1. The facility was filled with demineralized water at 70°F. The water was circulated through the 85-kW electrical heater under sufficient pressure to retain a liquid state throughout the facility. This procedure continued until the water in the blow-down vessel attained the required (predetermined) temperature.

2. The electrical heater was turned off, and circulation was continued to minimize any temperature stratification in the vessel. When a uniform temperature was obtained, circulation was halted and the vessel was isolated from the heating loop.

3. The experimental run was taken by opening the valve to the test section while pressurizing the vessel with nitrogen from the top. The nitrogen was supplied at a sufficient rate to maintain a constant vessel pressure, which was greater than the corresponding saturation pressure, thereby ensuring a liquid state in the vessel.

B. The Blow-down Vessel

The vessel was constructed from a 21-in.-ID steel cylinder, 180 in. long, with $2\frac{1}{2}$-in. walls. It could hold approximately 2000 lb of water and was hydrostatically tested to 2200 psi along with the rest of the basic apparatus.

C. Nitrogen System

The nitrogen system consisted of six nitrgoen bottles and two delivery lines. The low-flow delivery line was governed by a Victor

air regulator and was capable of maintaining the tank pressure to within ±1 psi. The high delivery system, used for large flow rates, was controlled by an air-driven, 1/2-in. Annin valve, which maintained the pressure to within ±2 psi.

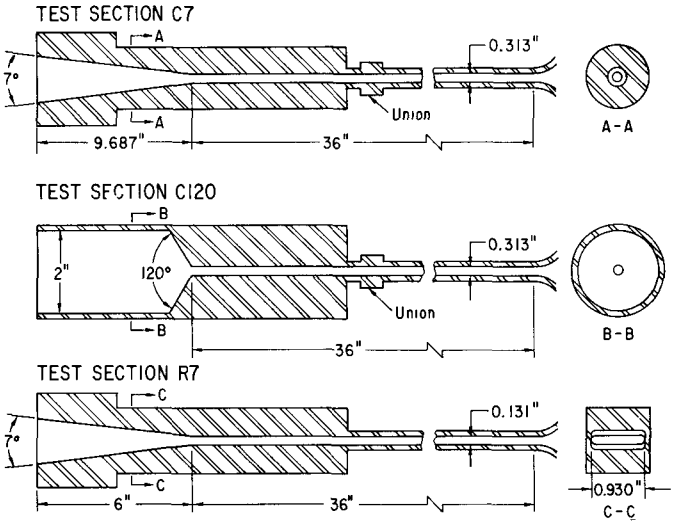

Fig. 4. Schematic Diagram of Test Sections Used in This Experiment, Showing Important Dimensions

D. Test Sections

Data from three test sections were obtained in this experimental investigation. The test sections were 36 in. long and constructed of Type 304 stainless steel. Figure 4 shows the test sections and their pertinent overall dimensions, and Table I lists the location of all pressure taps in each section. There was no readily available method for making the sections in one piece because of their length. Consequently, each test section was fabricated in two parts. The details of how the sections were constructed are given in Appendix A.

TABLE I. Pressure-tap Locations in Test Sections

Test Section C7			Test Section C120			Test Section R7		
Position	Distance from Exit Plane, in.	Accuracy of Pressure Measurement, psi	Position	Distance from Exit Plane, in.	Accuracy of Pressure Measurement, psi	Position	Distance from Exit Plane, in.	Accuracy of Pressure Measurement, psi
U8	+30.0	±2.0				U8	+30.0	±2.0
U7	+15.0	±2.0	U7	+30.0	±2.0	U7	+15.6	±2.0
U6	+6.0	±2.0	U6	+15.0	±2.0	U6	+6.0	±2.0
U5	+2.747	±2.0	U5	+6.0	±2.0	U5	+3.250	±2.0
U4	+1.498	±1.0	U4	+2.747	±2.0	U4	+2.000	±1.0
U3	+0.502	±1.0	U3	+1.500	±1.0	U3	+1.250	±1.0
U2	+0.032	±1.0	U2	+0.505	±1.0	U2	+0.687	±1.0
U1	+0.011	±1.0	U1	+0.031	±1.0	U1	+0.127	±1.0
Exit	0.000	±0.10	Exit	+0.010	±0.10	Exit	+0.010	±0.10
D1	-0.123	±1.0	D1	-0.001	±1.0	D1	-0.5	±1.0
D2	-0.500	±1.0	D2	-0.068	±1.0	D2	-1.0	±1.0
D3	-1.002	±1.0	D3	-0.129	±1.0	D3	-3.5	±1.0
D4	-2.5	±1.0	D4	-0.247	±1.0	D4	-5.0	±1.0

Test Sections C7 and C120 were made to investigate the effect of the downstream geometry on the critical-flow data. This effect is discussed in Chapter V. Test Section R7 was constructed for two reasons:

1. The different geometrical configuration enabled the effect of cross-sectional geometry on the critical flow rate to be studied.

2. The width of the channel (0.930 in.) provided a suitable empty-full ratio so that the gamma-ray attenuation technique for measuring void fractions would give reasonably accurate results.

E. Pressure Measurement

All pressure measurements, except for the exit pressure in the 40-60-psia range, were obtained using Bourdon-tube pressure guages, which were periodically calibrated against a dead-weight tester. The accuracy of each pressure measurement, for 40 psia $\leq P_e \leq$ 60 psia, is listed in Table I. The exit pressure in this range was determined by a 100-in. mercury manometer, which measured pressures accurate to within ±0.1 psi.

For experimental runs taken at exit pressures of 100 and 150 psia, the exit pressure was recorded by a Bourdon-tube gauge which was accurate within ±1.0 psi. For these runs, all pressure measurements other than the throat measurement were accurate to within ±2.0 psi.

The exit pressure was always measured by the upstream tap located closest to the exit plane. Test Section C120 had a 0.010-in.-diam pressure tap located 0.001 in. downstream of the throat. Since part of the tap was in a very low-pressure field, it was concluded that the tap would not produce a pressure representative of the exit plane. The measurement recorded by the wall tap located 0.010 in. upstream of the throat was used as the exit pressure for Test Section C120.

F. Flow-rate Measurement

Since the blow-down vessel was quite tall and the water in the tank was always maintained in a subcooled state, a convenient method for measuring the flow rate was to determine the time interval for a given head drop in the vessel. The time interval was measured with a stopwatch, and the head drop by a Statham ±5-psi differential pressure transducer, which was connected to pressure taps located at the bottom and top of the tank as shown in Fig. 3. The input signal to the transducer was provided by a Hewlett-Packard power supply, and the output was read on a four-digit Hewlett-Packard digital voltmeter. The head of nitrogen above the water was taken into account by assuming the nitrogen was at the same temperature as the water resulting in a 1-2% correction in the flow rate.

This method was checked by filling the tank with cold water and then blowing it down into a weight tank. The flow-rate measurement always compared with the weight-tank value within 2% and was usually within 1%.

The differential transducer was calibrated with a mercury manometer before and after each run.

G. Temperature Measurement

Two thermocouples were used in the blow-down system. A Chromel-Alumel thermocouple was used in the tank, and an iron-constantan thermocouple was used in the 1/2-in. pipe leading to the test section. Both were calibrated in a silicon oil bath using a platinum resistance thermometer as the standard. A Mueller bridge and a Leeds & Northrup galvanometer were used to determine the temperature of the platinum resistance thermometer, and the thermocouples were read on a Leeds & Northrup potentiometer.

During a test run, both thermocouples were recorded and agreement of $\pm 0.5°F$ was attained when the system was in a liquid state at both thermocouples. For the higher-quality runs ($x > 0.03$), the downstream couple was located in a two-phase mixture. Consequently, its temperature was lower than the tank temperature. In this situation, the tank couple was considered the stagnation temperature.

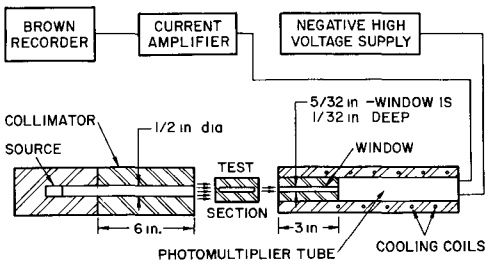

112-9296

Fig. 5. Apparatus Used to Measure Void Fractions

H. Void-fraction Measurement

Void fractions were measured by the gamma-ray attenuation apparatus shown in Fig. 5. The gamma-ray source was thulium-170, which has energy peaks at 84 and 52 keV and a half-life of 129 days.

Hooker and Popper[20] derived an expression relating the void fraction of a two-phase mixture and the attenuation of gamma rays beamed through such a mixture. This expression may be written as

$$\alpha = \ell n(\phi/\phi_f)/\ell n(\phi_0/\phi_f), \qquad (4\text{-}1)$$

where ϕ_0, ϕ_f, and ϕ are the empty, full, and two-phase signals, respectively.

The derivation for Eq. 4-1 is based on the premise that the attenuation of a gamma beam is an exponential function of the absorption thickness and the attenuation coefficient as shown in the following equation:

$$I = (I_0) \exp(-\mu y). \qquad (4\text{-}2)$$

The attenuation coefficient represents the summation of the beam attenuation due to scattering and absorption of the gamma rays, which for the gamma-ray energies characteristic of thulium-170 is 80% scattering and 20% absorption.[53]

The relationship given in Eq. 4-1 is based on two assumptions:

1. The gamma-ray beam is monoenergetic.

2. The beam is attenuated in series by the phases. (Series attenuation indicates that the gamma beam is perpendicular to distinct layers of each phase, as opposed to parallel attenuation where the beam is parallel to the layers of each phase.)

The sources available at Argonne National Laboratory are encapsulated in aluminum. Christensen[2] measured the energy spectrum of the encapsulated source. This spectrum is shown in Fig. 6. The gamma beam is far from being monoenergetic. However, Christensen also conducted an experiment to determine the variation in the gamma-ray signal to the detector as a function of the void fraction. His results show that the attenuation can still be described by a single absorption coefficient. Hence the formulation given in Eq. 4-1 still describes the void fraction.

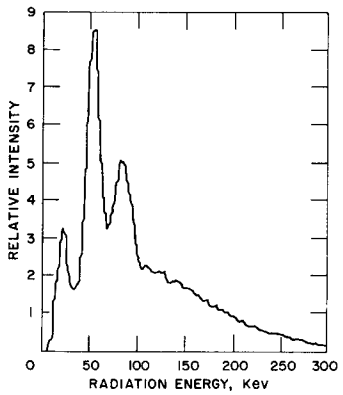

112-9575

Fig. 6
Gamma-ray Energy Spectrum[2]

Gouse[19] discussed the uncertainty of the gamma-ray attenuation technique due to the distribution of the phases. He showed that systems with large empty-to-full ratios as large as 10^2 are quite sensitive to the assumption of series or parallel attenuation. In this study, the empty-to-full ratio was rather small (1.3). Hence the degree of uncertainty was very small. The flow regimes witnessed at critical flow[14,46] appeared as thoroughly dispersed mixtures which are best represented by the series-attenuation model. Thus the degree of uncertainty was reduced even more. The lead collimator and detector window minimized the additional geometric effects described by Gouse.

Petrick and Swanson[39] described possible errors in the "one-shot" technique (the width of the detector window is wider than the channel) resulting from a point source and preferential phase distributions. These sources of error were eliminated by using a source that was wider than the channel.

The negative high voltage was supplied to the detector by an HVP5-61511 (500-1500 V) supply, and the detector was an RCA 6199 photomultiplier tube. The signal generated by the gamma beam was amplified by a Kiethley current amplifier and recorded on a Brown Electronik Recorder which had a 0.25-sec response time.

An error analysis for the gamma-ray attenuation using the above apparatus is presented in Appendix B.

CHAPTER V

DISCUSSION OF THE RESULTS

A. Validity of the One-dimensional, Steady-state Approach

The equations derived in Chapter III are based on the assumptions of one dimensionality and steady state. These assumptions are approximations to the real situation and are valid only in limited regions. For example, in single-phase flow, the one-dimensional approximation is valid only for high Reynolds numbers, where the velocity profile is almost flat. An investigation by Andeen and Griffith[1] indicated that an experimental justification of the one-dimensional and steady-state approximations was necessary before these assumptions could be used in any two-phase flow model.

Andeen and Griffith investigated these approximations for subcritical, two-phase, air-water flows. They measured the momentum flux by an impulse method and also measured the average void fraction in the test section by means of quick-closing valves. Their results show conclusively that, for low-velocity flows (small axial pressure gradients), the one-dimensional, steady-state momentum flux, which is calculated from the measured void fraction and quality, is considerably less than the measured flux This is illustrated in Fig. 7 where the measured momentum flux is compared to the predicted curves of the one-dimensional, steady-state model incorporating various values for the void fraction. The momentum multiplier used in Fig. 7 is defined in Ref. 1 as

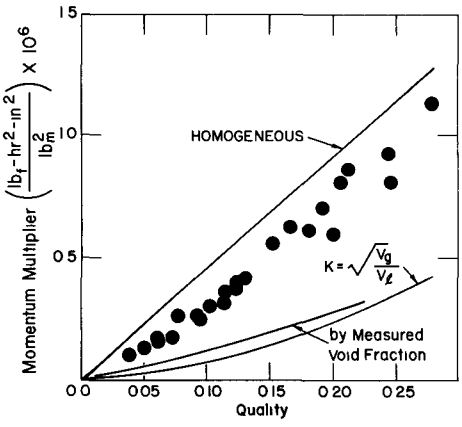

112-9313 Rev. 1

Fig 7 Air-Water Results of Andeen and Griffith[1]

$$MM = \frac{FORCE}{G^2A}.$$

Andeen and Griffith present three reasons for this deviation. (1) unsteady fluctuations such as slugging, (2) two-dimensional velocity profiles, and (3) turbulent fluctuations All the above reasons cause the real momentum to be greater than the one-dimensional, steady-state case.

Although the data and conclusions of Andeen and Griffith are quite valid at low velocities, their experimental apparatus contains possible errors for the high velocities characteristic of two-phase critical flow. Since the measured momentum flux is that of the exit plane, the exit void fraction is required to calculate the momentum efflux predicted under the one-dimensional, steady-state approximations The quick-closing-valve method of measuring void fractions gives an average void fraction over a

given axial length. This average void fraction is representative of the exit void fraction only when the momentum pressure drop is small compared to frictional pressure loss. When the momentum pressure drop is the predominant term in the momentum equation, as it is in critical flow, the quick-closing-valve technique is no longer a reasonably accurate method of obtaining the exit void fraction. Hence, in flows characterized by large axial pressure gradients, one must determine the exit void fraction before the one-dimensional approximation is advocated or condemned.

The total pressure drop is the summation of the momentum and frictional pressure drops when the head drop is negligible. That is, $\Delta P_T = \Delta P_M + \Delta P_f$.

If Eqs. 3-6 and 3-7 are substituted in Eq. 3-8, the momentum pressure drop for small-quality ($x_E < 0.02 \rightarrow$ momentum of the vapor $<<$ momentum of the liquid) flow may be expressed as

$$\Delta P_M = \frac{G^2 v_\ell}{g_c} \left(\frac{1}{1 - \alpha_2} - \frac{1}{1 - \alpha_1} \right). \tag{5-1}$$

Rose and Griffith[40] have shown that frictional pressure losses may be estimated by

$$\Delta P_f = f \frac{L}{D} \frac{\rho u_m^2}{2 g_c}, \tag{5-2}$$

where u_m is the homogeneous velocity,

$$u_m = \frac{G}{\rho_\ell (1 - \alpha) + \alpha \rho_g}, \tag{5-3}$$

and ρ is the two-phase density,

$$\rho = \alpha \rho_g + (1 - \alpha) \rho_\ell. \tag{5-4}$$

With the above equations, the total pressure drop, based on the one-dimensional, steady-state assumption, may be computed if the void fractions are known. This calculated pressure drop can then be compared with the actual pressure decrease to determine the validity of the assumed conditions.

In this work, the void fractions were measured by the gamma-ray attenuation technique at the exit plane and five positions upstream. The one-dimensional, steady-state pressure drop was then calculated by starting at the furthest point upstream and summing the momentum and frictional

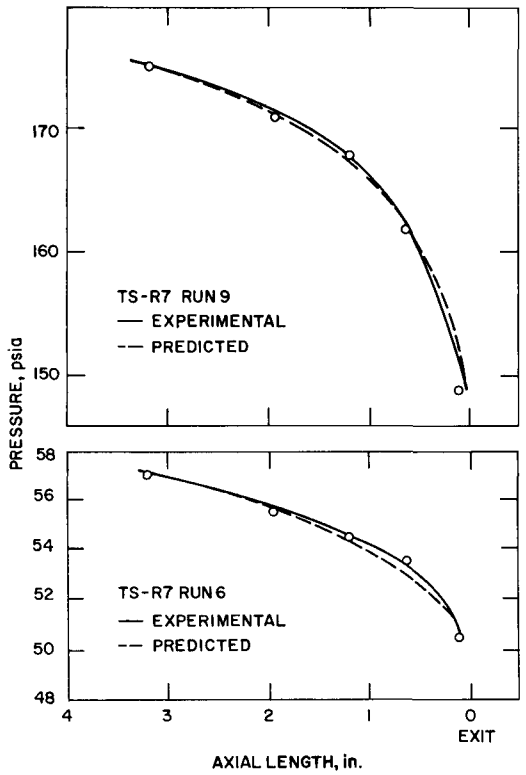

112-9293

Fig. 8. Comparison between Experimental Pressure Profiles and Those Predicted by Void-fraction Data

losses from point to point. The frictional losses were based on an average void fraction between the two points and an average friction factor of f = 0.020. The friction factor is actually a function of the Reynolds number as illustrated in Ref. 40. However, for the Reynolds numbers in this study (1.7×10^5-4.9×10^5), the experimental curve shown by Rose and Griffith would have to be extrapolated. Since the extrapolation would be questionable and the pressure-drop calculations showed the frictional losses to be only 10-20% of the total pressure drop, the above figure was chosen as a representative magnitude for the friction factor.

Figure 8 shows the agreement between the calculated and measured profiles for two runs of Test Section R7. Table II lists the measured and calculated total pressure drops between position U5 and the exit plane for all the runs of Test Section R7 where this type of void-fraction data was obtained. As is demonstrated by the graphs and the table, the agreement is quite good, indicating that a one-dimensional, steady-state approach reasonably approximates the physical situation for high-velocity flows.

TABLE II. Comparison between Measured and Calculated Total Pressure Drop

Run	ΔP_T, psi		% Deviation
	Measured	Calculated	
1	13.4	11.0	18
2	9.9	9.5	4
3	8.3	7.3	12
4	8.1	8.3	2
5	8.6	8.4	2
6	7.2	7.5	4
7	8.4	7.0	17
8	18.0	12.5	31
9	27.0	29.0	7

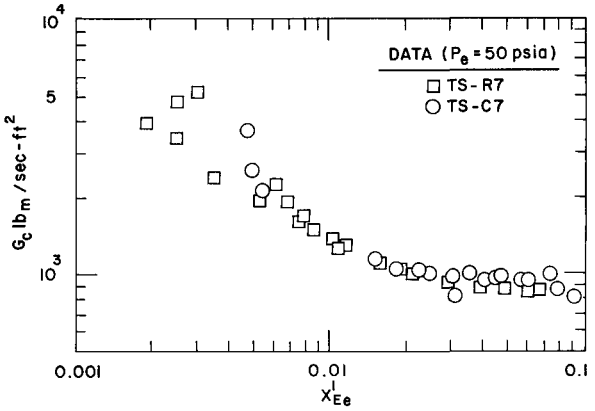

112-9311

Fig. 9. Comparison of Data for Test Sections R7 and C7

B. Geometrical Comparisons

Figure 9 compares the data of Test Sections R7 and C7 at 50 psia. The excellent agreement between the results of the two test sections indicates that the cross-sectional geometry of the channel (rectangular as opposed to circular) does not significantly influence the flow. This geometrical independence can be deduced as another experimental justification of the one-dimensional assumption, which substantiates the conclusion drawn in Section A of this chapter.

The small deviations between Test Sections R7 and C7 for $x_E > 0.03$ are discussed in Part F of this chapter.

C. Exit-pressure Measurement

Figure 10 demonstrates the theoretical behavior of the pressure profiles in a constant-area duct for subcritical and critical flows. The figure shows that when the receiver pressure is less than the throat pressure, the flow is choked, and under this condition, a perturbation in the receiver pressure does not affect the upstream pressure profile. One should be able to increase the receiver pressure from Point d to Point b without affecting any of the upstream conditions. At Point b, the receiver pressure is exactly equal to the throat pressure; this is the highest receiver pressure that will permit critical flow for given upstream stagnation conditions.

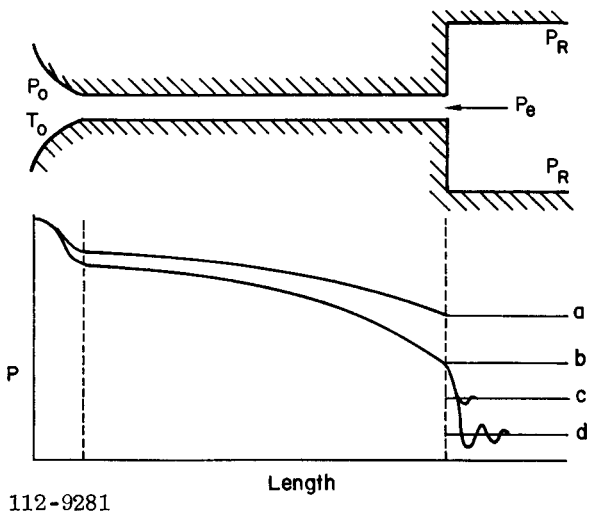

112-9281

Fig. 10. Theoretical Pressure Profiles for Subcritical and Critical Flows in a Constant-area Duct

Table III summarizes some of the two-phase critical-flow investigations discussed in Chapter II. Each investigation used a test section similar to the constant-area duct pictured in Fig. 10. However, the experimental pressure profiles differed from those shown in the figure. When the receiver pressure was increased from d to c, the exit pressure also increased.

TABLE III. Investigations Observing Exit-pressure Dependence

References	Testing Fluid	Test Section ID, in.	Critical Pressure, psia	Quality Range	Method of Obtaining Exit Pressure
Isbin et al.[21]	Water	0.374-1.04	4-43	0.01-1.0	Linear extrapolation for the last 1/2 in.
Faletti and Moulton[8]	Water	0.574	26-106	0.001-1.00	Probe
Zaloudek[49]	Water	0.520-0.625	40-110	0.004-0.99	Linear extrapolation for the last 1/32 in.
Klingebiel[29]	Water	0.500	28-53	0.01-0.99	Probe and a tap 0.005 in. upstream of exit

Isbin et al.[21] were the first to observe this dependency of the exit pressure upon receiver pressure. Their suggested explanation of this behavior was that a pressure disturbance could possibly propagate through a thin liquid annulus.

Faletti and Moulton[8] were the next to observe this phenomenon from measurements made with a probe that extended the length of the test section and out into the receiver. In effect, they measured the flow in an annulus. The pressure tap in the probe was perpendicular to the flow stream so that the static pressure was measured. By moving the tap up- and downstream of the exit plane, they could obtain a pressure profile through the exit plane. This technique for measuring the exit pressure also revealed a dependency on receiver pressure. Faletti and Moulton reasoned that the exit pressure in two-phase critical flow is not well defined, and that there is a maximum allowable expansion chamber pressure (MAECP) which, if exceeded, will cause the flow to become subcritical. Exceeding the MAECP will change the throat pressure or the flow rate or both. At qualities less than 50%, Faletti and Moulton found the MAECP to be less than the exit pressure for two-phase critical flows.

Zaloudek[49] performed essentially the same experiments as those described above, but instead of using a probe, he extrapolated linearly from a wall tap located 1/32 in. upstream of the exit plane. His results closely agreed with those of Faletti and Moulton.

Zaloudek used pressure transducers and an X-Y recorder to closely study the relationship between the exit and receiver pressures. His instrumentation indicated that for qualities less than 75% a large enough differential could not be produced between the exit and receiver pressures so that a further decrease in the receiver pressure did not result in a slight decrease in the exit pressure. This effect was observed even when the differential pressure was as large as 100 psi. This observation does not totally contradict the explanation presented by Faletti and Moulton, but

indicates that it is highly questionable because even at differential pressures of 100 psi across the exit plane, Zaloudek could not find an MAECP. Hence, if such a pressure exists, it must be extremely low. Zaloudek attributed his experimental observations to an asymptotic approach to critical flow.

Another investigator to witness the relationship between the exit and receiver pressures was Klingebiel.[29] He placed a wall tap within 0.005 in. of the exit plane and also used a probe to determine if any discrepancy existed between the two methods under critical-flow conditions. He found discrepancies between his probe and the wall-tap measurements in the last 0.10 in., indicating a radial pressure distribution near the exit. He attributed the discrepancies to a wall effect. However, the pressure measurements obtained by means of the probe are also influenced by the receiver pressure. This fact indicates that the probe is merely another wall which suffers from the same behavior as a tap on the outside wall, the magnitude of the effect being less.

All the studies discussed above used a constant-area test section expanding into an essentially infinite receiver, and each investigation indicated a dependency of exit pressure with receiver pressure. Since this dependency between the exit and receiver pressures is not predicted by a one-dimensional approach, a possible reason for this phenomenon is the two dimensionality of the flow at the exit plane.

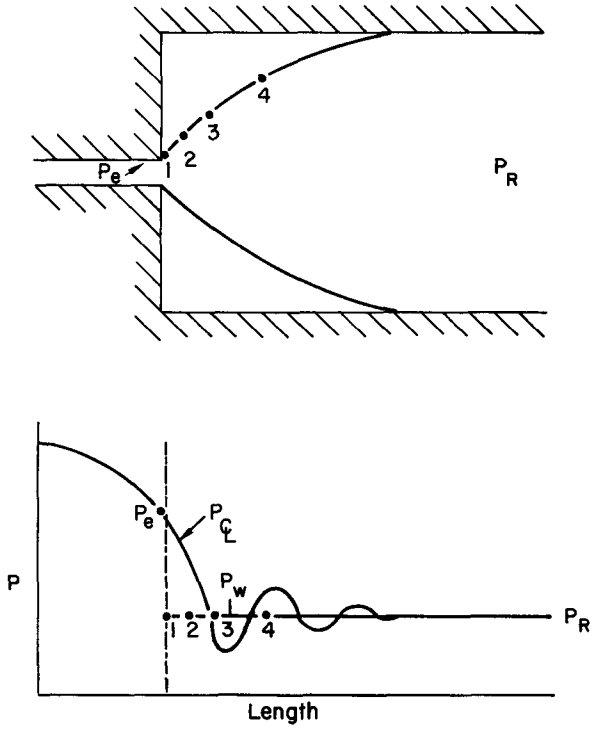

112-9295

Fig. 11. Two-dimensional Aspects of a Rapid Expansion

A critical-flow field that encounters an abrupt expansion separates from the walls and expands freely in shape of a "plume," as shown in Fig. 11. All jets entering an infinite medium will expand because of the viscous nature of the fluid. However, the expansion associated with critical flow occurs much faster than that resulting from a momentum exchange between the jet and the fluid occupying the infinite cavity. This rapid expansion must be a result of a radial pressure gradient, which implies the existence of a two-dimensional pressure distribution. This two-dimensional behavior is pictured in Fig. 11 where $P_{\mathbb{C}}$ is the depressurization along the centerline and P_w is that measured at the wall (which is the same as the surface of the plume). Figure 11 shows a discontinuity between P_e

and P_w, which cannot exist in the real case; there must be a continuous depressurization of the fluid near the wall. The fluid near the wall is subsonic, because of the zero velocity restriction at the wall; this should enable the receiver pressure to propagate upstream slightly. The upstream propagation will adjust the pressure distribution near the exit plane, resulting in a steep axial gradient along the wall and thus influencing the measurement recorded by a wall tap located very near the exit plane. The essence of this discussion is that if the pressure field is highly two-dimensional, a measurement recorded by a wall tap near the throat may not be at all indicative of the free-stream pressure for the same axial position.

The magnitude of the radial pressure gradient immediately downstream of the exit plane may be decreased by decreasing the angle of divergence of the walls to geometrically restrict the expansion of the fluid. If the magnitude of the radial pressure gradient in the vicinity of the exit plane is decreased, the pressure measurement recorded by a wall tap located near the exit will be more characteristic of the free-stream pressure for that axial position.

To determine if the two dimensionality of the flow field is a reason for the dependency between the exit and receiver pressures, two test sections were constructed. These two sections were hydrodynamically identical upstream of the exit plane, the only difference being their downstream geometry, which, according to the normal description of critical flow, should not affect the conditions at the throat.

Test Section C120 was a constant-area duct with a 120° included angle divergence at the exit plane. The large divergence resulted in an abrupt expansion of the flow field. Hence this section was essentially the same as those used by the previous investigators. Test Section C7 was also a constant-area duct, but it diverged from the exit plane at an included angle of 7°. This small divergence would still allow the flow to choke at the throat, but it would geometrically restrict the flow field downstream. Test Section R7, like Test Section C7, was a constant-area duct with a 7° included angle divergence but had a rectangular instead of a circular cross section.

All three test sections were operated at an exit pressure of 50 psia in the quality range $0.002 < x_{Ee} < 0.20$, and the results of the experiments, along with the data of Ref. 49 at 50 psia, are shown in Fig. 12. As shown by the figure, there is excellent agreement between the data of Ref. 49 and Test Section C120, and also between Test Sections C7 and R7. There are, however, distinct differences between the data taken with an abrupt expansion and those taken with a 7° expansion section.

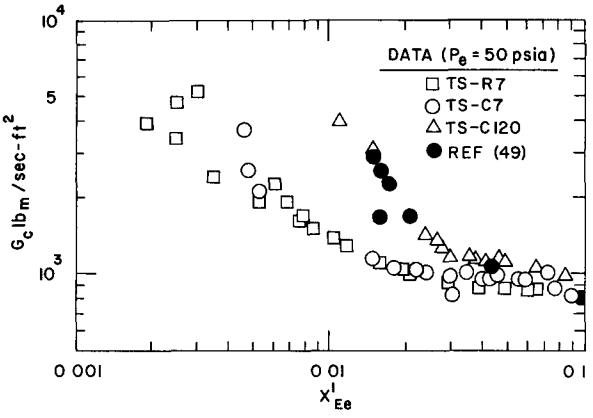

112-9312

Fig. 12. Comparison of Data for Different Downstream Geometries

If the differences exhibited in Fig. 12 are caused by different two-dimensional expansions at the exit plane, and if Test Section C7 reduces the magnitude of the radial pressure gradients, then the pressure profiles of Test Section C7 should be more closely allied with the normal one-dimensional explanation of critical flow than those of Test Section C120. Figure 13 shows the pressure profiles near the exit plane for Test Section C120 under two-phase critical-flow conditions. The dependency between the exit and receiver pressures is in agreement with the results of Refs. 8, 21, 29, and 49, which used similar geometries. Figure 14 shows the results of a similar test conducted with Test Section C7 for two-phase critical flow. If the downstream curve described by Run 12-A is considered the supersonic expansion for the 7° geometry, the characteristics of Test Section C7 are closely related to single-phase critical-flow behavior. In the single-phase case, successive increases in the back pressure result in moving the point of deviation from the supersonic curve closer to the exit plane until the point of deviation is coincident with the exit. A further increase in the back pressure will cause the exit pressure, until then fixed, to increase. This behavior is identical to that manifested by Test Section C7 for two-phase critical flow. The only difference between the single- and two-phase flow cases is the rate of departure from the supersonic curve. For single-phase flow the departure takes place in a sudden pressure rise, whereas in two-phase flow the departure

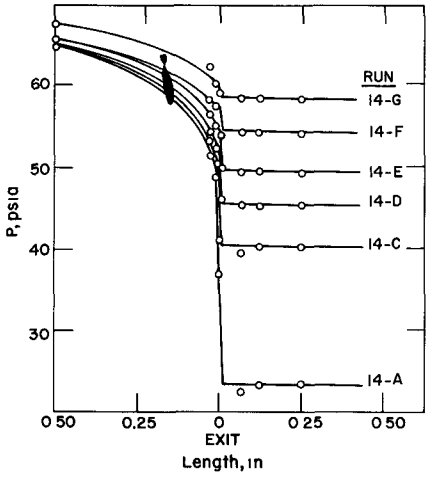

112-9288

Fig. 13. Dependency between Exit and Receiver Pressures for Test Section C120

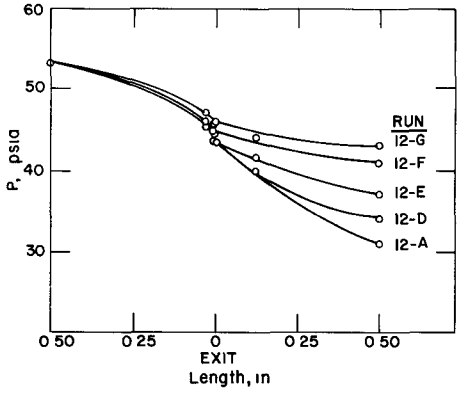

112-9282

Fig. 14. Exit-pressure Behavior for Test Section C7

is a gradually increasing deviation from the supersonic profile. This behavior for two-phase "shocks" was also recorded in Ref. 45, which investigated overexpanded nozzles in one-component, two-phase flow.

It is concluded from the evidence given in Figs. 13 and 14 that Test Section C7 will produce an exit pressure which is more characteristic of the free stream because it geometrically minimizes the magnitude of the inherent two-dimensional effects. Thus the data of Test Section C7 more closely represent the physical situation.

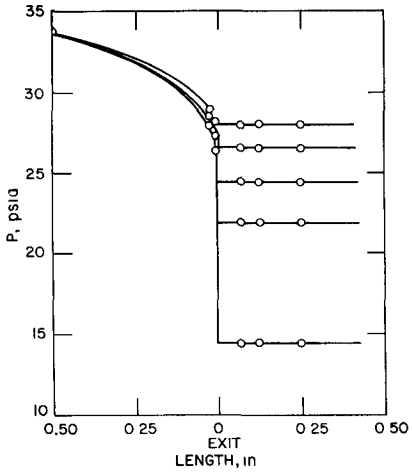

112-9289

Fig. 15. Single-phase Pressure Profiles for Test Section C120

The magnitude of this two-dimensional effect in single-phase critical flow was investigated by connecting a manometer between the exit wall tap and the first pressure tap downstream of the exit for both Test Sections C7 and C120. The test sections were put through the same procedure described above using nitrogen as the working fluid. The results, shown in Figs. 15 and 16, indicate that the discrepancy is still present although the magnitude of the effect is small. This observation substantiates the two-dimensional explanation rather than the descriptions of previous investigators[8,21,49] who assigned this behavior only to two-phase flows.

If the two dimensionality of the flow is the only cause for discrepancies in a rapid expansion, the effect should decrease as the receiver pressure increases and should reduce to zero at the point where the exit and receiver pressures are equal. This condition results in no radial expansion and thus no two-dimensional effects. Hence a wall tap located near the exit plane should produce a representative pressure under these circumstances. Analysis of the two-phase, one-component data presented by Klingebiel and those shown in Fig. 13 indicates that the flow may be subcritical when the exit and receiver pressures are not equal. Consequently, additional phenomena must be present in two-phase, one-component flow. The conditions that are most likely always present in two-phase, one-component critical flow are slip between the phases and a retarded phase change.

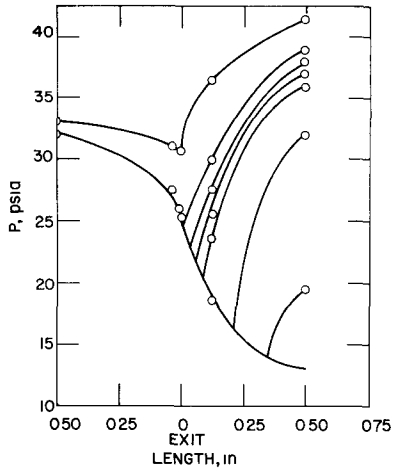

112-9308

Fig. 16. Single-phase Pressure Profiles for Test Section C7

If the exit and receiver pressures are equal, the exhausting fluid should appear as a

constant-area jet in a region near the exit plane. (The jet will spread further downstream because of a momentum exchange with the surrounding fluid.) For two-phase flows at low qualities, this constant area behavior is described by Eq. 5-1,

$$\Delta P_M = \frac{G^2 v_\ell}{g_c} \left(\frac{1}{1 - \alpha_2} - \frac{1}{1 - \alpha_1} \right), \tag{5-1}$$

where the viscous effects are considered small. The above expression clearly shows that if the pressure is constant (exit and receiver pressures are equal), the void fraction must also remain constant. The exiting fluid contains two nonequilibrium conditions: slip between the phases, and a nonequilibrium phase distribution which may relax toward equilibrium. The stable state that these two conditions approach is homogeneous equilibrium flow. The viscous nature of the fluid will reduce the velocity ratio from some value greater than one to unity, which implies an acceleration of the liquid and a deceleration of the vapor. This momentum interchange of the phases will increase the void fraction. A nonequilibrium, low-quality mixture will convert some superheated liquid into saturated vapor until the free energies of the phases are equal. This "flashing" of liquid into vapor will also increase the void fraction. The relaxation of each nonequilibrium state results in an increasing void fraction which, from Eq. 5-1, must be accompanied by a decreasing pressure. The decreasing pressure implies that the receiver pressure must be less than the exit pressure, and, thus, that there will be some radial expansion of the jet. Equation 5-1 only holds for constant-area flow. However, it illustrates the impossibility of such flows when the above-mentioned nonequilibrium conditions are present. The existence of these two states prevents the equality of the exit and receiver pressures <u>even when the flow is subcritical.</u> This is why two-phase, one-component systems may exhibit a pressure profile which is characteristic of critical flow by single-phase standards ($P_e > P_R$), and the flow is still subcritical. The relaxation of the two nonequilibrium states may also be one reason for the decreasing pressure profile in a diverging geometry under subcritical conditions as shown for Test Section C7 in Fig. 14.

Any system that does not experience the phenomenon described above should suffer only from the two-dimensional aspects of the expansion at the throat, which can be decreased by making the exit and receiver pressures nearly equal. Single-phase critical flow in an abrupt expansion should produce this situation. In Part E of this chapter, the relative importance of each of the nonequilibrium phenomena is discussed and evidence is presented to show that the velocity ratio is near unity for low-quality flows. If this is the case, air-water flows should not show much discrepancy between the exit and receiver pressures at the minimum receiver pressure for critical flow. Fauske[14] used this fact to determine the existence of critical flow in an air-water mixture; when the flow displayed an expansion at the exit, the system was choked at the throat.

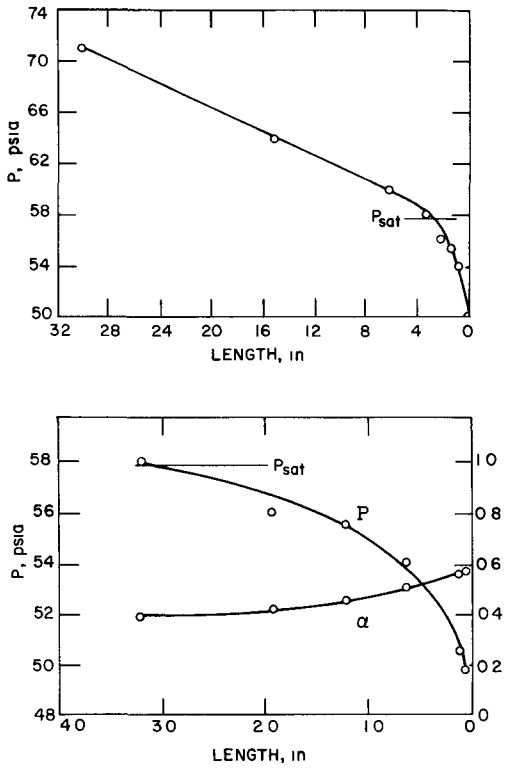

112-9294

Fig. 17 Pressure and Void-fraction Profiles for Run 3 of Test Section R7

D. Dissolved Gases

The data of Test Section R7, as shown by Fig. 17, exhibit two interesting aspects:

1. The pressure gradient deviates from the constant value characteristic of all liquid flow before the saturation pressure is reached.

2. The void fraction is greater than zero, which indicates the presence of a gaseous phase, when the static pressure is greater than the saturation pressure. (The saturation value was determined by measuring the temperature of the subcooled liquid in the blow-down vessel.)

The first point is indicative of acceleration, which can only be achieved if the system becomes compressible. Hence a gaseous phase must be present. The second aspect confirms the physical reasoning of the first.

Since the flow is adiabatic, the formation of a gaseous phase, at a pressure greater than the saturation pressure, cannot be due to subcooled boiling. Therefore this phenomenon must be a result of previously dissolved gases coming out of solution. The fact that boiling is nonexistent at these pressures does not negate the possibility of water-vapor formation. As the gases come out of solution, they may also carry water vapor in the form of humidity, and since the system pressure is very near the saturation value, a gaseous bubble existing at 100% relative humidity will be almost entirely composed of water vapor. In this capacity, the gases coming out of solution act as a source to create water vapor before boiling is initiated.

The experimental apparatus used in this study was not capable of de-aerating the water. However, Zaloudek[50] commented on the influence of dissolved gases in two-phase flow. He varied the amount of air dissolved in the water by heating the fluid in an open tank to 90°C; the decrease in the air content resulted in critical flow rates that were 5-8% greater.

Figure 18 shows that this study was not the only two-phase critical-flow investigation plagued by dissolved gases.[4,6,29] A close examination of the pressure profiles shows the flow was accelerating before reaching the saturation pressure, which means a gaseous phase was present.

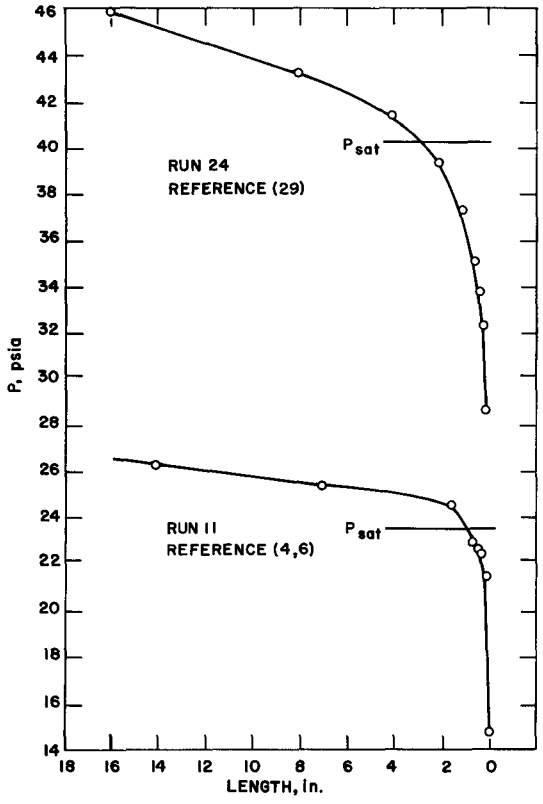

112-9302

Fig. 18. Experimental Data of Refs. 6 and 29, Indicating That Dissolved Gases Are Coming Out of Solution

The presence of a gaseous phase while the pressure is greater than the corresponding saturation pressure definitely affects the axial profile of the quantity N. Equation 3-24 indicates that if $\alpha > 0$ and $x_E = 0 (P < P_{sat})$, then N is infinite. Hence the variable N will begin at infinity and decrease to the exit value (as shown later in Fig. 24).

E. Comparison between Data and Theoretical Models

Figures 19-23 show the comparison between the author's theory, in its range of validity ($X_{Ee} < 0.02$), and the experimental data. (As a result of the conclusions in Part C of this chapter, neither the data of Test Section C120 nor that of previous investigators are used in the comparisons.)

Figure 20 also illustrates the predictions of previous models in the low-quality region. This behavior is characteristic of these models at all pressures shown. Hence, for clarity, the models are only displayed in Fig. 20. Two points are immediately obvious from Fig. 20:

1. As predicted by the theories of Levy[31] and Moody,[35] the experimental critical flow rates do not exhibit a maximum as a function of equilibrium quality.

2. None of the equilibrium theories predict the correct slope for the data in the low-quality region.

The slope of the data $(\partial G_c/\partial x_{Ee})_{P_e}$ in the low-quality region is an interesting quantity. The homogeneous equilibrium model and the equilibrium theories of Fauske,[9] Levy,[31] and Moody[35] demonstrate the result of assuming an equilibrium expansion. At low qualities, the slope $(\partial G_c/\partial x_{Ee})_{P_e}$ is approximately zero because of the predominance of the nearly constant equilibrium-phase-change term $v_g(\partial x_E/\partial P)_{H_0}$ in the critical-flow equation. The data exhibit a very large negative slope, and, as was discussed previously, the deviation from the homogeneous equilibrium theory must be due to slip between the phases, a retarded phase change, or both. If the phase

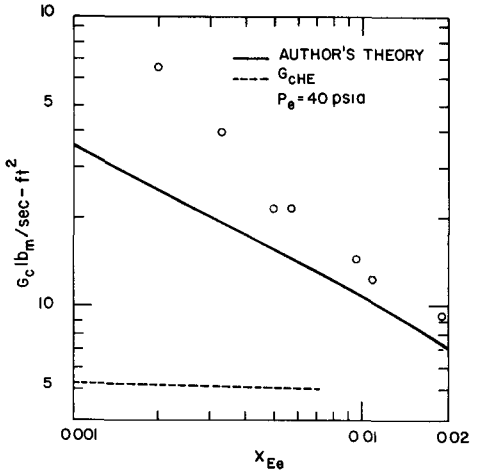

112-9283

Fig. 19. Comparison between Author's Theory and Experimental Data of Test Section C7 for P_e = 40 psia

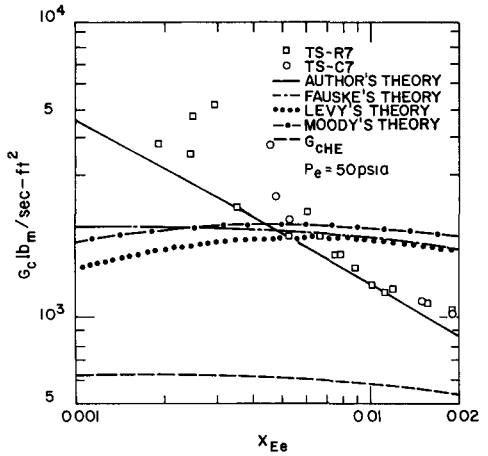

112-9280

Fig. 20. Comparison between Author's Theory, Equilibrium Theories of Refs. 9, 31, and 35, and Experimental Data of Test Sections C7 and R7 for P_e = 50 psia

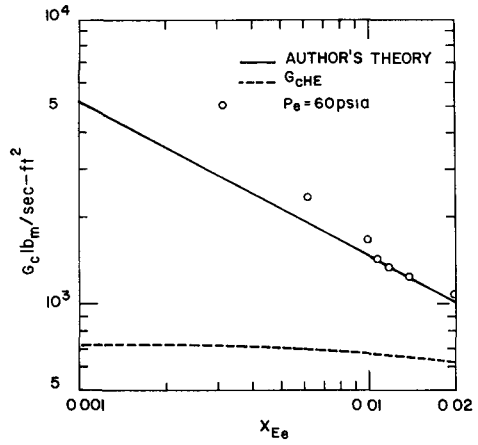

112-9284

Fig. 21. Comparison between Author's Theory and Experimental Data of Test Section C7 for P_e = 60 psia

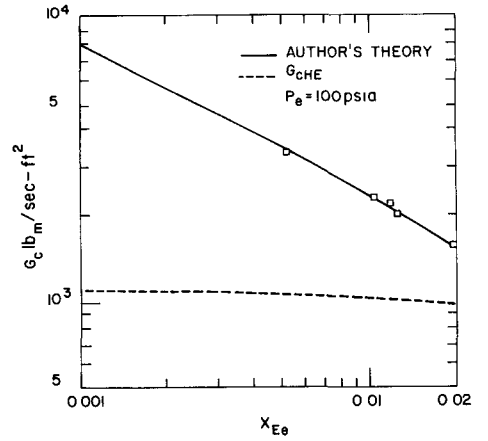

112-9286

Fig. 22. Comparison between Author's Theory and Experimental Data of Test Section R7 for P_e = 100 psia

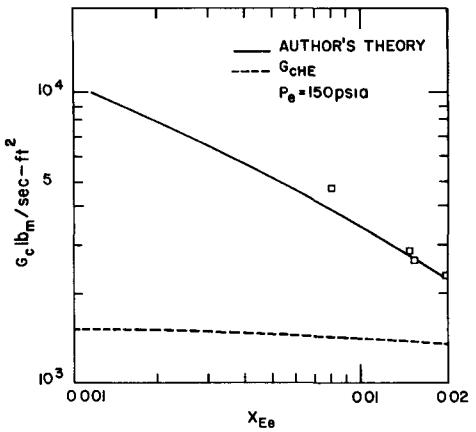

112-9285

Fig. 23

Comparison between Author's Theory and Experimental Data of Test Section R7 for P_e = 150 psia

change is assumed to be in an equilibrium state, then the deviation is due only to slip between the phases, in which case the large negative slope would indicate a velocity ratio that increased with decreasing quality and that $(\partial k/\partial P)_{H_0}$ would also behave in this manner. The term $(\partial k/\partial P)_{H_0}$ is representative of the momentum transfer between the phases. When its value is zero, the system transfers momentum between its phases at an infinite rate, as is the case in homogeneous flow. When the absolute value of this term is large, little momentum is transferred, which is the case for droplet or mist flows. In the quality range reported here, the flow regime is far removed from mist flow and probably is in some form of bubbly flow. For gaseous bubbles entrained in a liquid, one would expect rather large rates of momentum transfer, and as the quality decreases, the bubble size also decreases so that the transfer rate increases. The implication of the above discussion is that it does not appear reasonable to expect that $(\partial k/\partial P)_{H_0}$ will increase with decreasing quality. In fact, one would probably expect the opposite to occur. If one assumes that the velocity ratio is near unity, the deviation from the homogeneous equilibrium model would then be mostly a result of a nonequilibrium phase change. For a phase change to occur, the system must be in a nonequilibrium state, which implies that all real phase changes are of a nonequilibrium nature. Thus the question becomes one of the magnitude of the phase change and not its nature. As was mentioned above, at low qualities ($x_{Ee} < 0.02$), the phase change $v_g(\partial x_E/\partial P)_{H_0}$ dominates the compressibility of the mixture. Hence any misrepresentation of the real process, such as an assumption of an equilibrium phase change, may result in large discrepancies between an analytical model and the real phenomenon. Since the mass transfer is of a nonequilibrium nature and its formulation is so critical at low qualities, it is quite plausible that the deviations between G_{cHE} and the data are mainly due to a retarded phase change. If this is the case, the degree of retardation must increase with decreasing quality. At higher qualities ($x_{Ee} > 0.20$), the representation of the mass transfer is not so crucial and the equilibrium assumption will not affect a theoretical model to any great degree.

The prediction of Eq. 3-25 shows good agreement with the data for $x_{Ee} < 0.02$ and $P_e \geq 50$ psia. For these limits, the data are within 20%, except for the points at very low qualities where the problem of dissolved gases causes tremendous scatter. The agreement between the theory and the data indicates that the assumptions made in Chapter III are reasonable approximations to the physical conditions. In particular, the assumptions that N_e is not a function of the exit pressure and that $(\partial N/\partial P)_{H_0} = 0$ apparently are not greatly different than the real process. For $P_e = 40$ psia, the theoretical prediction considerably underpredicts the critical flow rates. However, it does exhibit a slope similar to that of the data.

At moderate void fractions ($0.30 < \alpha_e < 0.80$) and higher pressures ($P_e \geq 50$ psia), the theory shows best agreement with the data. This is not

unexpected since $(\partial N_e/\partial P_e)_{H_0}$ includes the term $(\partial k_e/\partial P_e)_{H_0}$. At lower pressures, where the density ratio becomes larger, the magnitude of $(\partial k_e/\partial P_e)_{H_0}$ may become greater and thus destroy the interplay with $(\partial x_e/\partial P_e)_{H_0}$ which produced the approximation that $(\partial N_e/\partial P_e)_{H_0} = 0$. At very low qualities ($x_{Ee} < 0.005$), the scatter in the data becomes appreciable and the experimental flow rates are 0-100% greater than the author's theory. The scatter appears to be a result of varying amounts of dissolved gases exiting from solution. At very low qualities, these gases could occupy a considerable portion of the recorded void fraction. The void fractions were used to obtain N in a manner that assumed all the voidage was occupied by steam, and the resulting correlation was used as if only steam and water existed in the channel. It was shown in Part D of this chapter that the actual system contains steam, water, and air. The theoretical development assumed that air was a negligible quantity compared with x_e. However, if it was not, the system would be less compressible than proposed by the theoretical model because the air experiences only a density change and lacks the additional compressibility induced by a phase change. Such a decrease in the compressibility would result in a higher flow rate. Hence the air content could cause the discrepancies between the author's theory and the experimental data. Figure 24 shows that the upstream gradients of $(\partial N/\partial P)_{H_0}$ are much steeper at low void fractions than those shown in Fig. 2 for higher values of voidage. Hence the approximation that $(\partial N_e/\partial P_e)_{H_0} = 0$ appears to be somewhat worse at the lower void fractions. The illustrations of Fig. 24 show the slope $(\partial N_e/\partial P_e)_{H_0}$ to be positive, which produces a larger flow rate as shown by Eq. 3-22. Thus the behavior of the derivative is in agreement with the higher experimental flow rates. The breakdown of the assumption $(\partial N_e/\partial P_e)_{H_0} = 0$ could also result from the presence of a considerable amount of air in the system.

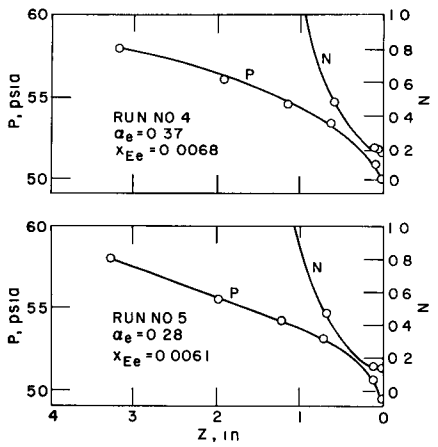

Fig. 24. The Slope $(\partial N/\partial P)_{H_0}$ for Low Void Fractions

Figure 25 compares the author's theory and experimental data in the void-fraction region, which was the area of principal interest. The error

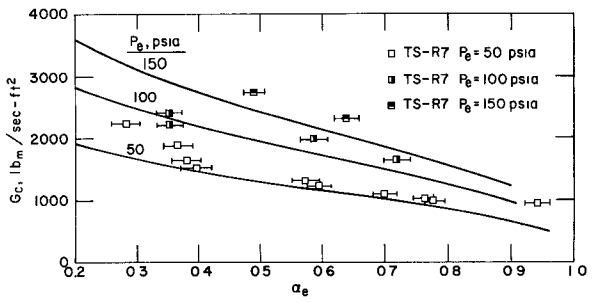

Fig. 25

Comparison between Author's Theory and Experimental Data in Void-fraction Region

in the void-fraction measurement (which is discussed in Appendix B) is illustrated by the error bars. The maximum error in the flow-rate measurement, as discussed in Chapter IV, is smaller than the size of the data points. The good agreement verifies the usefulness of the theory in calculating critical flow rates for the void-fraction range ($0.30 < \alpha_e < 0.80$) and exit pressures in the range ($50 \text{ psia} \leq P_e \leq 150 \text{ psia}$). Figure 26 demonstrates the pressure independency of the G_c/G_{cHE} ratio as given by Eq. 3-26.

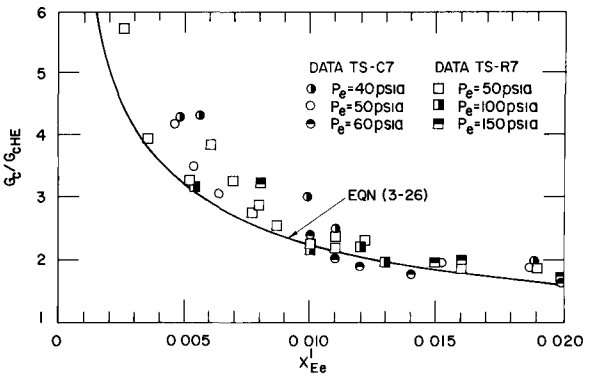

112-9306

Fig. 26. Comparison between Theoretical Prediction of G_c/G_{cHE} and Experimental Data for all Exit Pressures

Figure 27 compares the theory for two-component, two-phase critical flow at low qualities with the experimental data of Ref. 14. The theoretical prediction is based on the experimental velocity ratios listed in Table IV. The derivation of Eq. 3-29 assumed that $(\partial k_e/\partial P_e)_{H_0} = 0$ is an asymtotic solution that becomes more exact at lower void fractions. As illustrated in Fig. 27, this reasoning is validated by the experimental results. The derivative $(\partial k_e/\partial P_e)_{H_0}$ certainly cannot be equal to zero in the region of steep pressure gradients (critical flow) when the phases have such widely different densities as air and water do. However, the quantity should diminish in importance as the void fraction becomes very small, thus exhibiting the asymtotic approach to the theory shown in Fig. 27. An empirical relationship for the velocity ratio is presented in Ref. 14, and theoretical approaches are presented in Refs. 14 and 6 which differentiate this correlation to evaluate $(\partial k/\partial P_e)_{H_0}$. Note that this correlation is incorrect because it is a summation of exit velocity ratios for different flow rates and stagnation enthalpies and hence does not represent the physical situation, which is $(\partial k/\partial Z)_{H_0}/(\partial P/\partial Z)_{H_0}$ evaluated at the exit plane. The derivative $(\partial k/\partial P_e)_{H_0}$ can only be evaluated when the behavior of k near the exit plane has been determined.

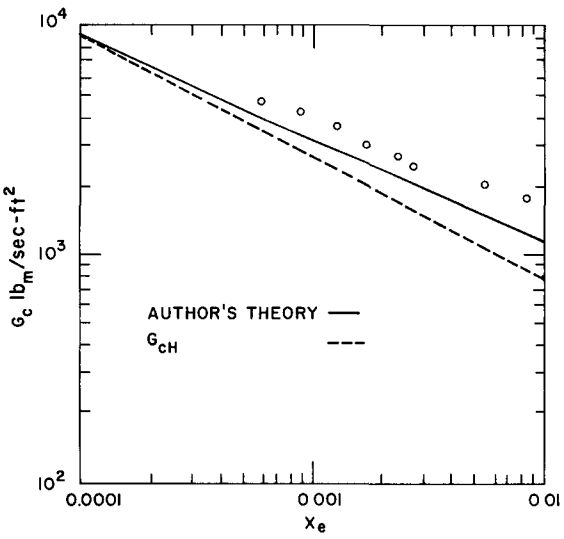

112-9300

Fig. 27. Comparison between Two-component Asymptotic Theory and Experimental Data of Ref. 14 for P_e = 17 psia

TABLE IV. Critical Flow Data for a 0.123 x 1.0-in. Lucite Channel; Critical Pressure, P_c = 17 ± 0.25 psia[14]

Quality, x	Void Fraction, α	Velocity Ratio, k	Flow Rate G_c, $lb_m/sec\text{-}ft^2$
0.00060	0.277	1.13	4500
0.00087	0.336	1.24	4000
0.00126	0.405	1.33	3300
0.00173	0.474	1.39	3100
0.00235	0.528	1.51	2800
0.00276	0.558	1.58	2600
0.00568	0.689	1.85	2100
0.00885	0.768	1.95	1800
0.0130	0.817	2.13	1600
0.0177	0.860	2.11	1450
0.0334	0.913	2.38	1100
0.0827	0.964	2.39	640

F. General Observations

Faletti and Moulton[8] and Zaloudek[49] observed that the experimental ratio of G_c/G_{cHE} was independent of pressure for qualities greater than 20%. For $0.02 < x_{Ee} < 0.15$, a pressure dependency was evident in both investigations. However, they differ on the shape of the curves in this quality region. Although the low-quality region was the area of principal interest in this study, the range of qualities was extended to include this phenomenon.

Figure 28 shows the behavior of G_c/G_{cHE} in the quality range of interest. As was shown in Fig. 12, there is excellent agreement between Zaloudek's data and that of Test Section C120. The discrepancies between Test Sections C120 and C7 are most likely due to erroneous pressure measurements, as discussed in Part C of this chapter, and hence should be the reason for the differences manifested in Fig. 28. Figure 29 shows the pressure dependency observed in this research, which is a suppression of G_c/G_{cHE} with increasing pressure. Figures 28 and 29 show a definite "hump" in the data of Test Section C7 in the neighborhood of $0.05 < x_{Ee} < 0.08$. This "hump" was also observed by Faletti and Moulton; however, the magnitude

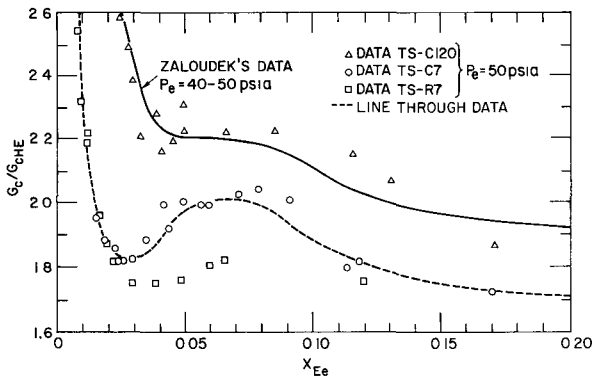

112-9304

Fig. 28. Comparison of G_c/G_{cHE} for Different Geometries

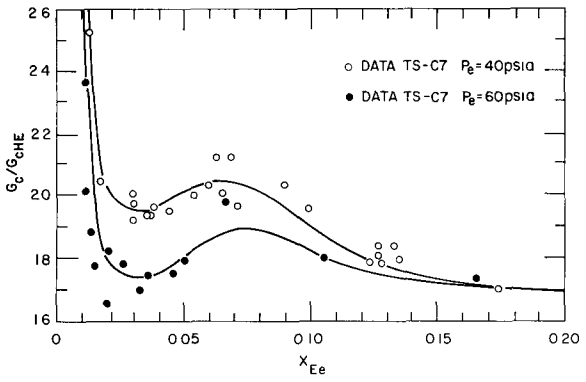

112-9305

Fig. 29. Pressure Dependency of G_c/G_{cHE}

of their ratios was slightly greater than that of Zaloudek's. It is of interest to investigate possible reasons for this "hump." Fauske[14] showed that air-water critical flow also exhibited this behavior in the region of x = 0.05, as is shown in Fig. 30. The experimental data of Ref. 14 also reveal that the velocity ratio appears to reach a maximum in the same region. Klingebiel[29] measured velocity ratios in a steam-water system at qualities of 0.02-1.0 and found that the velocity ratio decreased with increasing qualities. The magnitude of the measurements in Ref. 29 may be in error because of possible erroneous exit-pressure measurements and nonequilibrium phase changes. However, at rather high qualities ($x_{Ee} > 0.20$), these effects should be small, and one should be able to rely upon the trends of the data. The velocity-ratio data of Refs. 14 and 29 are shown in Fig. 30. Although the results of Klingebiel and Fauske were obtained in different systems and at different pressures, they should reveal the behavior of k_e as a function of the exit quality. Comparing the slopes $(\partial k_e/\partial x_e)_{P_e}$ for each investigation shows that the velocity ratio exhibits a maximum in the neighborhood of $0.04 < x_e < 0.10$. In the critical-flow equation, Eq. 3-17, the velocity ratio is the only variable in the numerator, and although one cannot presently specify the exact behavior of the denominator, a maximum in the velocity ratio should produce a maximum in the G_c/G_{cHE} ratio. The pressure dependency shown in Fig. 29 is the same as that of the velocity ratio; the ratio is suppressed with increasing pressure.

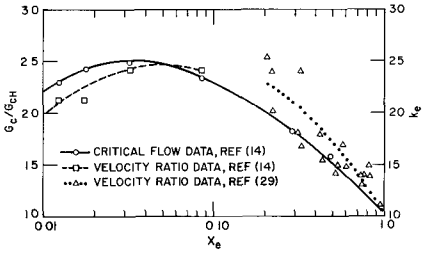

112-9291

Fig. 30. Experimental Evidence of a Maximum Velocity Ratio for a Given Exit Pressure

Based on the above observations, the "humps" shown in Figs. 28-30 appear to be characterized by a maximum velocity ratio for a given exit pressure.

Fauske's air-water data approached the homogeneous model as the quality decreased from 1% to zero. However, Fig. 28 shows a rapid divergence from the homogeneous equilibrium model for low-quality steam-water data. As was discussed in Part E of this chapter, this rapid divergence of the one-component data is a result of either increasing slip between the phases or a retarded phase change. For low-quality air-water

flows, the velocity ratio and $(\partial k/\partial P)_{H_0}$ both decrease with decreasing quality as is evidenced by the velocity ratios reported in Ref. 14 and the results of Fig. 27; hence, it appears that this rapid divergence is a result of a retarded phase change.

Figure 9 showed the good agreement between Test Sections C7 and R7 for $x_{Ee} < 0.03$. However, for $x_{Ee} \geq 0.03$, the agreement is not too good, as is shown by Fig. 28. This lack of agreement is because Test Section C7 was machined on a lathe and thus has a well-defined throat, while Test Section R7 was formed by an electrical-discharge machine that produced an exit plane that was not so well defined. As a result, the throat-pressure tap for Test Section R7 was located upstream of the actual throat. A pressure greater than the throat pressure was therefore recorded at this pressure tap. At low qualities ($x_{Ee} < 0.03$), the pressure gradients are comparatively gradual. Hence the resulting effect was small. However, at higher qualities, the steeper gradients caused discrepancies between the data. On this basis, Test Section C7 more closely represents the physical condition in the quality range $x_{Ee} > 0.03$.

Several investigators[8,29,49] witnessed oscillatory pressures in critical flows at low qualities. They attributed this behavior to the existence of "slug flow" in the test section. These oscillations were not observed in this research. The studies that witnessed this phenomenon created the two-phase fluid by mixing cold water and superheated steam. For low-quality flows, the pressure in the mixing chamber may be higher than the saturation pressure of the mixture. This higher pressure causes the steam to condense rapidly. Such condensation usually produces pressure oscillations, such as those experienced in cavitation studies, and these oscillations may propagate downstream and disturb the pressure measurements in the test section. The only oscillations observed in this investigation occurred at higher qualities where it was necessary to "flash" in the upstream valve, and the oscillations induced by this process propagated downstream.

The lack of pressure oscillations at low qualities further substantiates the steady-state approach discussed in Part A of this chapter.

G. Slip between the Phases and Retarded Phase Change

Slip between the phases and the effects of retarded phase change are considered together here because of their interdependency, which is evident from the following equation:

$$k = \frac{x}{1 - x} \frac{1 - \alpha}{\alpha} \frac{v_g}{v_\ell}. \tag{5-5}$$

This may be approximated to

$$k = x \frac{1 - \alpha}{\alpha} \frac{v_g}{v_\ell}$$

when $(1 - x) \approx 1$. When the density ratio and void fraction are determined experimentally, the actual velocity ratio can only be calculated when the real quality is known. If an equilibrium expansion is assumed, the equilibrium quality may be determined, and thus an "equilibrium velocity ratio" may be calculated on this basis. Figure 31 shows the equilibrium velocity ratios experimentally obtained in this study along with those obtained using several theoretical models. If the phases of a low-quality "flashing" flow are not in equilibrium, then $x < x_E$, which indicates that the actual velocity ratio is less than the value based on the equilibrium assumption. As discussed in Part A of this chapter, the pressure decrease near the throat in critical flow is essentially due to an increase in momentum of the fluid. In such a flow field, where the wall friction is negligible and the pressure gradient is negative, the velocity ratio should be greater than unity. Hence the velocity ratio is bounded by the "equilibrium velocity ratio" and unity. These bounds indicate that the data point for $\alpha_e = 0.94$, $k_{Ee} = 1.3$, shown in Fig. 31 has an actual velocity ratio between 1.0 and 1.3. All the points in Fig. 31 may be bracketed in this manner. However, the point listed above has the closest bounds. Since the value of actual velocity ratio is known within 30% for this particular point, it will be used as a reference point to examine one component velocity ratios in light of previous data.

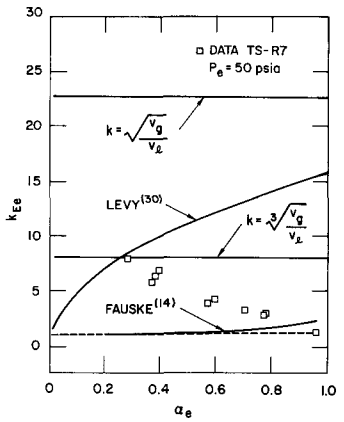

112-9301 Rev. 1

Fig. 31

Comparison between Experimental Equilibrium Velocity Ratios and Theoretical Models for P_e = 50 psia

The correlation set forth in Ref. 14 is based on measured void fractions in air-water, two-phase critical flows. Since a two-component mixture was used, the quality could be measured. Therefore the actual velocity ratio could be calculated based on experimental values of α_e and P_e. These results indicate that the velocity ratio decreases with decreasing void fraction in the range $0.27 \leq \alpha_e \leq 0.91$, and also show that the magnitude of the velocity ratio is within the range $1.0 \leq k_e \leq 2.5$. Fauske[14] contends that the exit velocity ratios of an air-water mixture are greater than or equal to those of a steam-water mixture with the same quality and density ratio. This is based on the reasoning that a one-component mixture must accelerate not only the existing vapor, but the newly formed vapor as well, whereas a two-component system only accelerates the existing gaseous phase. Although not much data has been accumulated on this subject, what has been taken appears to agree with the above reasoning. For instance, in Ref. 14, $x = 0.033$, $\rho_\ell/\rho_g \approx 700$, and $k_e = 2.4$; and in this study, $x_{Ee} = 0.039$, $\rho_\ell/\rho_g \approx 500$, and $k_{Ee} = 1.3$. Although the density ratios are not the same, they are close enough to suggest that the above reasoning is valid.

The experimental observation[14] that the velocity ratio decreases as the void fraction decreases is not unexpected. As the void fraction decreases, the system tends to become one of gaseous bubbles entrained in liquid, and one would not expect velocity ratios much larger than unity.

It has been shown in this chapter that:

1. The variables k and $(\partial k/\partial P)_{H_0}$ both decrease with decreasing quality for low-quality air-water flows.

2. In the quality region where the mass transfer does not dominate the compressibility of a one-component mixture, air-water and steam-water mixtures exhibit a similar behavior in that both display a maximum of G_c/G_{cHE} as a function of quality for $x_{Ee} \approx 0.07$. This maximum is apparently the result of a maximum of the velocity ratio as a function of quality.

3. The meager data available indicate that the velocity ratios of a steam-water mixture are less than those for one composed of air and water.

It has been argued that:

4. Phenomenologically, one would expect k and $(\partial k/\partial P)_{H_0}$ to decrease with decreasing quality for low-quality steam-water mixtures.

The four summary points listed above imply that (1) $(\partial k_e/\partial x_{Ee})_{P_e} > 0$, and (2) the air-water velocity ratios are greater than those of steam-water mixtures. As discussed previously, one knows the actual velocity ratio of the reference point within 30%. Hence, if one postulates a curve representing the behavior of the actual exit velocity ratios, it should start at the reference point and follow the behavior patterns described above. Such a curve is shown by the dashed line in Fig. 31. This line shows only qualitative effects and contains no quantitative information. However, if the exit velocity ratio of the reference point ($k_{Ee} = 1.3$) is the maximum exit velocity ratio in the range investigated, then the exit velocity ratios are always near unity for low-quality flows. More directly stated, this implies that low-quality flows are nearly homogeneous.

Based on the above conclusion, the deviation between the "equilibrium velocity ratios" and unity is primarily due to a retarded phase change. In fact, this deviation can be used as an indication of the amount of superheat present in the liquid.

H. A Proposed Mechanism for One-component, Two-phase Critical Flow at Low Qualities

Part C of this chapter showed experimentally (Fig. 14) that the exit-plane pressure in two-phase critical flow exhibits a behavior that closely resembles that of the single-phase case. Part D concluded that the velocity ratios in the void-fraction range $0.0 < \alpha_e < 0.90$ are very close to unity. The existence of a nonequilibrium phase change in the flow field was deduced in Parts D and F.

In light of the above evidence, the following mechanism is proposed for one-component, two-phase critical flow in the void-fraction range $0.20 < \alpha_e < 0.90$:

1. The fluid is choked at the throat because of the existence of a sonic-velocity condition.

2. This sonic velocity is characteristic of the system compressibility which is determined by (a) the bulk modulus of each phase, (b) the velocity ratio, (c) the rate of change of the velocity ratio $(\partial k_e/\partial P_e)_{H_0}$, (d) the quality, which is less than the thermodynamic equilibrium value, and (e) the phase change $(\partial x_e/\partial P_e)_{H_0}$, which is nonzero but less than the thermodynamic equilibrium value.

The homogeneous equilibrium sonic velocity, which corresponds to the homogeneous equilibrium critical-flow model derived in Chapter III, may be expressed as

$$a_{HE}^2 = -g_c v_{HE}^2 \left(\frac{\partial P}{\partial v_{HE}}\right)_S, \tag{5-6}$$

where

$$v_{HE} = (1 - x_E)\, v_\ell + x_E v_g. \tag{5-7}$$

Substituting Eq. 5-7 into Eq. 5-6 and using the order-of-magnitude approximations used in Chapter III produces

$$a_{HE}^2 = \frac{-g_c[(1 - x_E)\, v_\ell + x_E v_g]^2}{x_E\left(\frac{\partial v_g}{\partial P}\right)_s + v_g\left(\frac{\partial x_E}{\partial P}\right)_s}, \tag{5-8}$$

so that

$$a_{HE} = G_{cHE} v_{HE}. \tag{5-9}$$

Semenov and Kosterin[44] developed a homogeneous sonic velocity which assumed that no phase change occurs $(\partial x/\partial P)_{H_0} = 0$ as the pulse travels through the mixture. They also assumed that the polytropic exponent of the vapor was equal to the ratio of the specific heats of vapor. Their expression may be written as

$$a^2_{HFZ} = \frac{[(1 - x_E)\, v_\ell + x_E v_g]^2}{x_E v_g^2}\, a^2_g. \tag{5-10}$$

The relationship of Eq. 5-10 is often called the homogeneous frozen model, and it exhibits the same trends as the sonic-velocity data given in Ref. 44, as shown in Fig. 32. The homogeneous frozen model appears to underestimate the data shown.

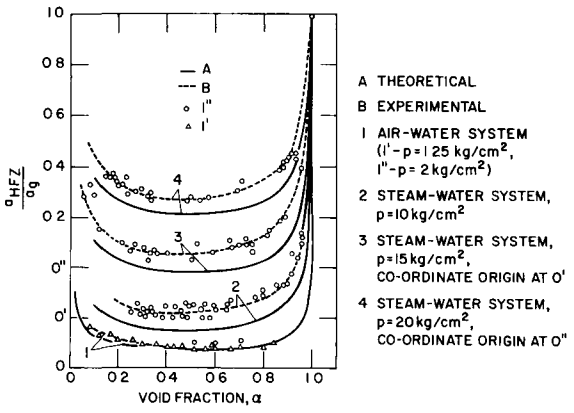

Fig. 32

Experimental and Theoretical Values for Two-phase Sonic Velocity[44]

112-9303 Rev. 1

It is argued in this report that the velocity ratios characteristic of low-quality, one-component, two-phase, critical flow are close to unity. Hence the specific volume of the mixture may be approximated by

$$v_H = (1 - x)\, v_\ell + x v_g = (1 - N x_E)\, v_\ell + n x_E v_g. \tag{5-11}$$

If Eq. 5-11 reasonably approximates the actual condition, and if the mechanism is the same for single- and two-phase critical flow, then the sonic velocity associated with two-phase critical flow at low qualities may be expressed as

$$a_c = G_c v_{He}. \tag{5-12}$$

Substituting Eq. 3-25 for the critical flow rate into Eq. 5-12 gives

$$a^2_c = \left\{ \frac{-g_c[(1 - x)\, v_\ell + x v_g]^2}{N\left[\dfrac{x_E v_g}{P} + v_g\left(\dfrac{\partial x_E}{\partial P}\right)_s\right]} \right\}_e \tag{5-13}$$

or

$$a_c = \left\{ \frac{v_H}{v_{HE}} \frac{a_{HE}}{\sqrt{N}} \right\}_e . \qquad (5\text{-}14)$$

The three sonic velocities discussed above are shown in Figs. 33-35 for three different pressures. The figures show that Eq. 5-13 exhibits characteristics of both the equilibrium and frozen models. For instance, (1) Eq. 5-13 appears to have a minimum velocity as does the frozen model, and (2) a change of phase occurs as in the equilibrium case; however, it is only a partial phase change.

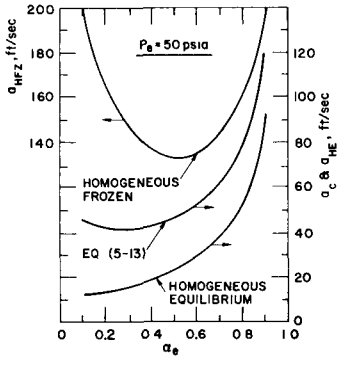

112-9314

Fig. 33

Homogeneous Sonic Velocities for One-component, Two-phase Flows at P_e = 50 psia

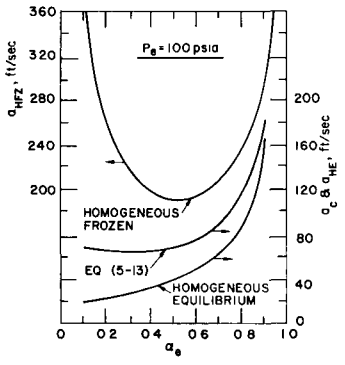

112-9315

Fig. 34

Homogeneous Sonic Velocities for One-component, Two-phase Flows at P_e = 100 psia

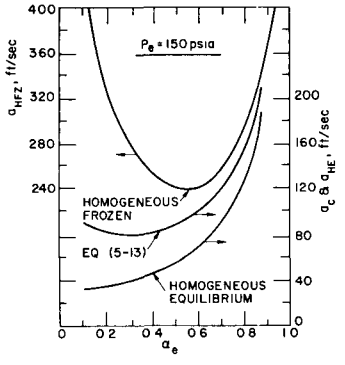

112-9316

Fig. 35

Homogeneous Sonic Velocities for One-component, Two-phase Flows at P_e = 150 psia

In single-phase flow, there is good agreement between the propagation velocity of small pressure pulses and the throat velocity experienced in critical flow. Comparing the same quantities in one-component, two-phase flow, one finds that the velocities differ by at least a factor of two. This result is not surprising when the compressibilities of the systems are considered. For single-phase gas flow, the compressibility is a function of the temperature only; hence, if the throat temperature in critical flow and the system temperature for a sonic pulse are equal, the velocities will be equal. As shown by Eq. 3-17, the compressibility of a one-component, two-phase mixture is a function of

$$\left(\frac{\partial P}{\partial \rho}\right)_{H_0} = F\left[v_g, \left(\frac{\partial v_g}{\partial P}\right)_{H_0}, x, \left(\frac{\partial x}{\partial P}\right)_{H_0}, k, \left(\frac{\partial k}{\partial P}\right)_{H_0}\right]. \qquad (5\text{-}15)$$

In their experiment, Semenov and Kosterin propagated a small pulse through an equilibrium mixture, whereas, in this study a high-velocity stream was choked at the throat. For the same pressure and stagnation

enthalpy, the terms v_g and $(\partial v_g/\partial P)_{H_0}$ are probably similar for each system. The steady-state velocity ratio k, and its derivative could conceivably be the same in each case. The main difference between these two systems is the phase change. In the experimental trials of Ref. 44, the pulse propagated through the equilibrium steam-water mixture with essentially no phase change, whereas, in low-quality, one-component critical flow, a sizable phase change appears to occur at the throat. This phase change is not an equilibrium process. Rather, it is one characteristic of considerable superheat in the liquid phase and is determined by the rate processes of heat and mass transfer upstream of the throat. Hence, the two systems discussed differ in the phase-change process, which is the controlling quantity at low qualities as shown by the difference between the equilibrium and frozen models. The data given in Ref. 44 are characteristic of a compression wave moving through a steam-water mixture. Such a pulse tends to create a subcooled liquid and a superheater vapor which are both stable conditions by themselves. Hence the mass transfer can occur only at the previously determined phase boundaries. For a rarefaction wave, which is more characteristic of critical flow, the unstable conditions of superheated liquid and supersaturated vapor are produced. Under these conditions, the liquid can "flash" and the vapor can condense. Therefore the systems can transfer mass independently of the previous phase boundaries. This indicates that compression and rarefaction sonic pulses may have different propagation velocities, and each of these may differ from the choking velocity in two-phase critical flow.

In summary, the pressure profiles suggest that a two-phase fluid behaves much like a single-phase medium; hence, a sonic velocity mechanism is proposed. The velocity ratio appears to be near unity and the phase change is neither zero nor the equilibrium value. Therefore a homogeneous partial-phase-change sonic velocity was proposed as an approximate mechanism for the phenomenon of low-quality, one-component, two-phase, critical flow.

CHAPTER VI

SUMMARY AND CONCLUSIONS

One-component, two-phase critical flows at low qualities were investigated analytically and experimentally. The mathematical model developed approximates the nonequilibrium processes by thermodynamic equilibrium paths. The model exhibits good agreement with the experimental data for $x_{Ee} \leq 0.02$ and 50 psia $\leq P_e \leq$ 150 psia. The theoretical prediction underestimates the critical flow rates for lower pressures and higher qualities. However, it exhibits the same slope $(\partial G_c/\partial x_{Ee})_{P_e}$ as the data at low qualities and $P_e < 50$ psia. The deviation that exists between the model and the data is a result of the approximation that $(\partial N_e/\partial P_e)_{H_0} = 0$.

It was argued that the exit velocity ratios in low-quality, one-component critical flows are not much larger than unity and that the phase change at these low qualities is a nonequilibrium process. Based on these arguments, a homogeneous, nonequilibrium sonic-velocity condition is proposed as the approximate mechanism for one-component, two-phase critical flow at low qualities.

An analysis of the experimental data leads to the following conclusions:

1. Axial-pressure and void-fraction measurements appear to justify the assumptions of one dimensionality and steady state for high-velocity, two-phase flows.

2. Comparison of the resulting data of Test Sections C7 and C120 indicated that previously reported data involve exit pressures that are not characteristic of the choking phonomenon due to the inherent two-dimensional behavior of a rapid expansion. The errors are particularly noticeable for $x_{Ee} < 0.10$.

3. The exit-receiver pressure relationship for all three test sections leads to the conclusion that the exit pressures of Test Sections C7 and R7 are more representative of the critical condition because the downstream two-dimensional effects are reduced by the geometry.

4. Comparing the axial void-fraction and pressure profiles reveals that a compressible phase is present when the pressure is greater than the saturation pressure corresponding to system temperature. This phenomenon is believed to be a result of previously dissolved gases exiting from solution. These gases also provide a source for vapor formation, in the form of humidity, before the inception of "flashing."

5. The "equilibrium velocity ratios" reported are the maximum ratio for a given pressure and void fraction. However, even these were smaller than the theoretical predictions.[9,31,35] This indicates that, although the critical-flow theories proposed in Refs. 9, 31 and 35 display good agreement for $0.01 < x_{Ee} < 1.00$, they do not correctly define the physical processes.

6. The experimental flow rates do not exhibit a maximum in a plot of G_c versus x_{Ee} as predicted by the theories of Refs. 31 and 35.

7. A comparison between the characteristics of one- and two-component critical flows reveals trends in the one-component systems that strongly suggest the existence and, for some conditions, the predominance of a retarded phase change.

8. The "hump" witnessed by Faletti and Moulton[8] was also observed in this study. Based on the velocity-ratio data of Fauske[14] and Klingebiel,[29] a maximum of the velocity ratio as a function of the quality was proposed as a possible explanation for the "hump."

CHAPTER VII

RECOMMENDATIONS FOR FUTURE STUDIES

A homogeneous, metastable, sonic-velocity mechanism was proposed in this study. This is only an approximation to the real case because in a real system the velocity ratio will be greater than unity and the derivative $(\partial k_e/\partial P_e)_{H_0}$ will be nonzero. If the problem of two-phase critical is to be understood, the mechanism of the critical condition must be clearly set forth. To do this, one must answer such questions as:

1. Is two-phase critical flow the result of a sonic-velocity condition at the throat?

2. If it is a sonic-velocity mechanism, how does one mathematically represent the various compressibility terms, $(\partial v_g/\partial P)_{H_0}$, $(\partial x/\partial P)_{H_0}$, and $(\partial k/\partial P)_{H_0}$, of the system?

3. If the phenomenon is due to a sonic condition, which, if either, of the phases travels at this velocity?

These are difficult questions to answer. However, a logical starting point would be a study of two-component, two-phase critical flows in a geometry similar to Test Section R7. This study should include axial void-fraction profiles so that the term $(\partial k_e/\partial P_e)_{H_0}$ may be investigated. Such efforts should also be accompanied by a thorough investigation of the velocity of sound in a two-component mixture. If the mechanism can be deduced for two-component flows, then the same mechanism will apply to one-component flows with the further complication of specifying the additional compressibility resulting from a change of phase.

APPENDIX A

Construction of the Test Sections

As was discussed in Chapter IV, the length of the test sections made it impossible to construct them from one piece of steel. Therefore the constant-area section was fabricated in two parts.

Test Sections C7 and C120 shared the same upstream portion, which was made from a 1/4-in. Schedule 80 pipe 32 in. long, whose ID was enlarged to 0.313 in. by polishing it out with emery paper. The OD was machined to 0.437 in. for the last $1\frac{1}{16}$ in. of the length.

The last 4 in. of the constant-area section and the downstream geometry of both Test Sections C7 and C120 were accurately bored on a lathe. The ID was drilled out to 0.313 in., and the OD was cut down to 0.437 for the first 39/64 in. of the sections.

The up- and downstream sections were joined by a stainless steel union, which was modified as shown in Figs. A.1 and A.2. The female portion of the union was common to both exit sections, but since each section had its own male part, there were actually three pieces to the union. Each part of the union was bored out to a diameter of 0.438 in. The exit section of Test Section C7 was inserted into its half of the union until its upstream face was flush with the surface of the union, where it was clamped and welded. The union was then joined, and the upstream portion of the test section was slid into its union half until it butted against the exit section where it was also clamped and welded. The union was disengaged and the female portion was joined with the male of Test Section C120. The exit section of Test Section C120 was inserted until it butted against the upstream section; there it was clamped and welded to its union half.

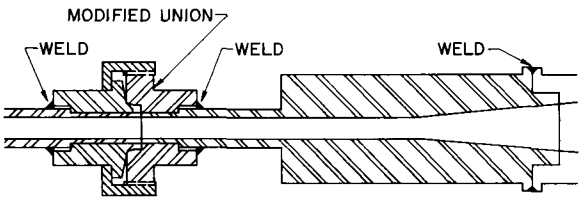

112-9299

Fig. A.1. Assembly of Test Section C7

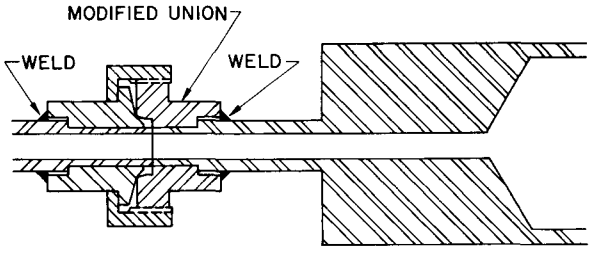

112-9297

Fig. A.2. Assembly of Test Section C120

To be certain no large deformations were caused by this procedure, the pressure profile was obtained for liquid flow only in each test section. A linear profile was observed in all cases.

The downstream divergence of Test Section C7 was continued by attaching an additional 8-in.-long section, which had the same angle of

divergence and ID at the joint as the exit section. The two parts were welded together at a point removed from the junction to minimize the distortion of the inner surface.

Test Section R7 was also constructed from two pieces. The upstream section was formed by squeezing a 3/4-in.-OD, 1/16-in.-wall circular tubing which resulted in the cross-sectional geometry shown in Fig. 4 The dimensions of the flow passage were constant within 0.002 in. The downstream section was constructed using an electrical-discharge machine (EDM) to form the channel to the same cross-sectional geometry as that of the upstream portion. These two pieces were then socket-welded together. The downstream geometry of Test Section R7 was extended by welding an additional nozzle onto the exit section. This was done before the final layer of metal was removed from the channel so that the last machine pass would form a smooth surface at the junction. As before, the pressure profile was determined for Test Section R7 with liquid flow only, and all trials yielded linear profiles. Hence the construction technique did not produce any large distortions of the channel.

During the experimental test with Test Section R7, the upstream section was backed up with 1/2-in. steel plates so it would not deform under internal pressure.

The pressure taps near the exit plane in all the test sections were formed by an EDM in order to: (1) accurately locate the taps, (2) precisely control their diameter, and (3) eliminate burrs. Table V lists the diameter and method used to install each pressure tap.

TABLE V. Characteristics of Pressure-tap Installation

Test Section C7			Test Section C120			Test Section R7		
Position	Diameter, in.	Method of Installation	Position	Diameter, in.	Method of Installation	Position	Diameter, in.	Method of Installation
U8	1/16	Drilled				U8	1/16	Drilled
U7	1/16	Drilled	U7	1/16	Drilled	U7	1/16	Drilled
U6	1/16	Drilled	U6	1/16	Drilled	U6	1/16	Drilled
U5	1/16	Drilled	U5	1/16	Drilled	U5	0.031	EDM
U4	0.010	EDM	U4	1/16	Drilled	U4	0.031	EDM
U3	0.010	EDM	U3	0.010	EDM	U3	0.031	EDM
U2	0.010	EDM	U2	0.010	EDM	U2	0.031	EDM
U1	0.010	EDM	U1	0.010	EDM	U1	0.031	EDM
Exit	0.010	EDM	Exit	0.010	EDM	Exit	0.031	EDM
D1	0.010	EDM	D1	0.010	EDM	D1	0.031	EDM
D2	0.010	EDM	D2	0.010	EDM	D2	0.031	EDM
D3	0.010	EDM	D3	0.010	EDM	D3	1/16	Drilled
D4	1/16	Drilled	D4	0.010	EDM	D4	1/16	Drilled

The details of the assembly of Test Sections C7, C120, and R7 are shown in Figs. A.1-A.3. Important dimensions of the test section were indicated in Fig. 4.

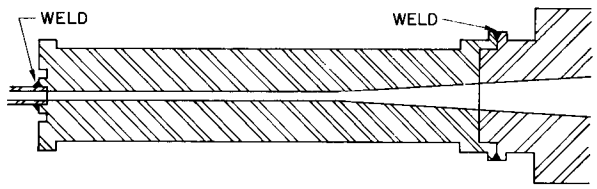

Fig. A.3
Assembly of Test Section R7

112-9298

APPENDIX B

Error Analysis of Gamma-ray Equipment

A thorough error analysis for the gamma-ray attenuation technique is presented in Ref. 20. Several sources of error are discussed and evaluated, but some of the errors are negligible in this investigation. The sources of error and their relationship to this system are listed below.

1. Errors resulting from electronic drifting of the current amplifier and the negative high-voltage supply and those due to the decay of the radioactive source were negligible because the time lapse for a run was approximately 15 min, which is very short compared with the time necessary for appreciable drift. The system was operated continuously to eliminate transients, and it was calibrated before, and checked after, each run to eliminate the influence of long time drifting.

2. Errors may result from external parallel radiation paths. However, the stainless steel of the test section, above and below the channel, negated this source of error for all practical purposes.

3. Errors arising from preferential phase distribution were dealt with in Chapter IV.

4. The gain of the photomultiplier tube is a function of the environmental temperature. Cooling coils were used to maintain a constant temperature around the tube. The temperature of the water supply was monitored, and a maximum variation of ±2°F was determined between different days. However, no fluctuations could be observed in the time required for a run. Therefore this source of error was also assumed to be negligible.

5. The Brown Electronik Recorder could be read to within 0.1 mV, compared to 30.0 mV for the full-scale reading. This is the only error listed in Ref. 20 that applies to this system.

As shown in Chapter IV, the void fraction may be represented by

$$\alpha = \frac{\ell n \frac{\phi}{\phi_f}}{\ell n \frac{\phi_0}{\phi_f}}. \qquad (4\text{-}1)$$

If empty and full measurements are taken at the same time, the ratio ϕ_0/ϕ_f is independent of drift and decay; it is only a function of the test-section geometry. This ratio was averaged for many readings, and the average

was used to calculate all the void fractions. Hence it may be considered a constant C_{efr} so that Eq. 4-1 becomes

$$\alpha = \frac{\ell n \frac{\phi}{\phi_f}}{\ell n\, C_{efr}}. \tag{B-1}$$

To obtain an appreciation of the errors involved, one would like to evaluate $\Delta\alpha/\alpha$. In Ref. 20, $\Delta\alpha$ is represented by $d\alpha$ (which only is valid when the errors are small) as

$$d\alpha = \frac{\frac{d\phi}{\phi} - \frac{d\phi_f}{\phi_f}}{\ell n\, C_{efr}} \tag{B-2}$$

or

$$\Delta\alpha = \frac{\frac{\Delta\phi}{\phi} - \frac{\Delta\phi_f}{\phi_f}}{\ell n\, C_{efr}}. \tag{B-3}$$

The maximum error is

$$\Delta\alpha = \frac{\frac{\Delta\phi}{\phi} + \frac{\Delta\phi_f}{\phi_f}}{\ell n\, C_{efr}}.$$

The errors in reading the strip chart are the same for ϕ as for ϕ_f. Hence $\Delta\phi = \Delta\phi_f$, or

$$\frac{\Delta\alpha}{\alpha} = \frac{\Delta\phi}{\alpha\phi_f\, \ell n\, C_{efr}} \left(\frac{\phi_f}{\phi} + 1\right). \tag{B-4}$$

The above formulation is permissible for small errors. However, when the errors become large it will produce error magnitudes that are not characteristic of the system.

For an error such as that created by misreading the strip chart, the erroneous void fraction may be represented by

$$\alpha_i = \frac{\ell n \frac{\phi + \Delta\phi}{\phi_f + \Delta\phi_f}}{\ell n\, C_{efr}}. \tag{B-5}$$

The variations $\Delta\phi$ and $\Delta\phi_f$ are of the same magnitude, and the maximum error will occur when they are opposite signs, for which

$$\alpha_i = \frac{\ell n \dfrac{\phi + \Delta\phi}{\phi_f - \Delta\phi_f}}{\ell n\, C_{efr}}. \qquad \text{(B-6)}$$

Also,

$$\frac{\Delta\alpha}{\alpha} = \frac{\alpha - \alpha_i}{\alpha} = 1 - \frac{\alpha_i}{\alpha} = 1 - \frac{\ell n \dfrac{\phi + \Delta\phi}{\phi_f - \Delta\phi_f}}{\ell n \dfrac{\phi}{\phi_f}}. \qquad \text{(B-7)}$$

This relationship holds regardless of the magnitude of the errors.

The two relationships are compared in Fig. B.1, and it is readily apparent that there are large differences in their predictions when the errors are sizable. The two methods converge for regions of small errors, which is in agreement with the derivation of Eq. B-4. Equation B-7 is a more exact formulation of the maximum possible error.

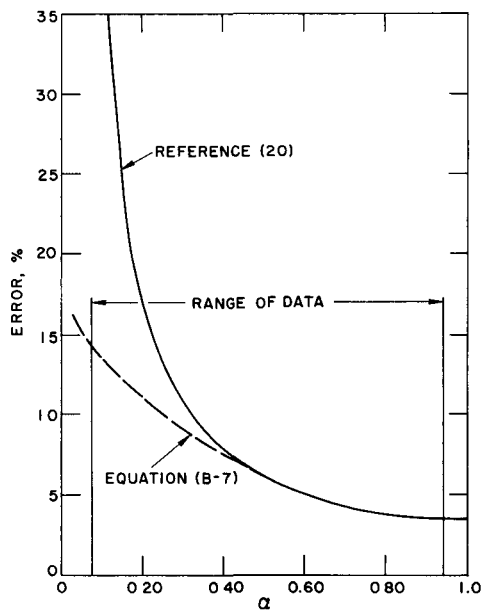

Fig. B.1

Maximum Percent Error in Void-fraction Measurements

APPENDIX C

Evaluation of the Thermodynamic Equilibrium Quality

Test Sections C7 and C120 were completely insulated with a 1-in. layer of fiber glass insulation to minimize the heat losses to the ambient. To facilitate the gamma-ray attenuation measurements, the exit section of Test Section R7 was not insulated. The heat losses from this test section were estimated by assuming the test section was at the temperature of the steam-water mixture and by assuming a heat-transfer coefficient of 5 Btu/hr-ft^2-°F. The estimated losses were 0.0007% of the heat content of the mixture. Since this value is so small and the losses of Test Sections C7 and C120 are even smaller because of their insulation, all the experimental runs were assumed to be adiabatic.

The energy equation for adiabatic flow may be written as

$$H_0 = h_\ell + xh_{fg} + \frac{G^2}{2g_c J}\left[\frac{x^3 v_g^2}{\alpha^2} + \frac{(1-x)^3\, v_\ell^2}{(1-\alpha)^2}\right]^2. \qquad \text{(C-1)}$$

If an equilibrium state is assumed, the pressure at a point fixes h_ℓ, h_{fg}, v_ℓ, and v_g. The stagnation enthalpy is constant for adiabatic flow and can be evaluated by knowing the temperature of the water when it is subcooled. G is the measured flow rate. This leaves Eq. C-1 with two unknowns, x and α. It was pointed out in Chapter III that the only type of flow in thermodynamic equilibrium is a homogeneous equilibrium flow. If H_0, G, and P_e are experimentally determined for a given flow, one will calculate the equilibrium quality only when a homogeneous flow is assumed. In essence, one is measuring parameters characteristic of a nonequilibrium state, but when the process is forced to equilibrium by assumption, the only flow model that may be used is the homogeneous one. Homogeneous flow simplifies Eq. C-1 to

$$H_0 = h_\ell + x_E h_{fg} + \frac{G^2}{2g_c J}(v_f + x_E v_{fg})^2. \qquad \text{(C-2)}$$

A knowledge of H_0, G, and P_e now enables one to determine the thermodynamic equilibrium quality x_E.

The quality calculated by the above method is only a reference value pertaining to a given state determined by the irreversible processes of metastability and slip between the phases. In the true sense of thermodynamic equilibrium in adiabatic flow, the quality must lie between the values determined by an isentropic and an isenthalpic expansion from the initial state (saturated liquid in this report) to the given pressure. Since the above formulation uses experimental values that are characteristic of a nonequilibrium state, the above expression may violate the Second Law of Thermodynamics; i.e., it may produce a quality less than that corresponding to an isentropic expansion. Therefore, the quality obtained from Eq. C-2 is only a reference value acquired by assuming that the flow at a point is in thermodynamic equilibrium.

APPENDIX D

Experimental Data

TABLE VI Critical-flow Data and Exit Parameters for Test Section C120

Run	H_0, Btu/lb$_m$	G_c lb$_m$/sec-ft^2	Exit Parameters P_e psia	Exit Parameters x_E	G_c/G_{cHE}
1	272 1	3126	54 0	0 015	5 00
2	316 9	1062	50 0	0 065	2 23
3	366 3	855	48 7	0 112	2 14
4	339 6	1000	50 9	0 084	2 23
5	425 6	685	50 5	0 168	1 86
6	300 7	1115	50 4	0 049	2 22
7	287 6	1126	50 0	0 038	2 15
8	277 4	1269	49 9	0 028	2 38
9	279 4	1168	49 8	0 030	2 20
10	277 1	1365	50 1	0 027	2 49
11	273 6	1427	49 8	0 024	2 62
12	285 5	1168	49 4	0 036	2 25
13	391 3	783	48 8	0 135	2 07
14	290 0	1115	49 0	0 041	2 19
14-A	289 7	1111	49 0	0 041	2 18
14-B	289 5	1115	49 5	0 040	2 19
14-C	289 5	1100	50 5	0 039	2 11
14-D	289 1	1100	52 5	0 036	2 01
14-E	288 8	1092	54 9	0 034	1 91
14-F	288 3	1107	57 5	0 030	1 78
14-G	288 0	1089	60 5	0 027	1 60
15	267 6	2185	50 1	0 016	3 79
16	267 5	2542	49 9	0 016	4 51
17	297 3	1153	49 6	0 047	2 32
18	268 9	2505	50 8	0 016	4 36
19	264 3	4068	50 7	0 011	6 91

TABLE VII Pressure Profiles (psia) for Test Section C120

Run	Position U7	U6	U5	U4	U3	U2	U1	Exit	D1	D2	D3	D4
1	97	83	76	72	70 0	68 0	57 0	54 0	39 5	25 0	23 0	23 0
2	124	112	97	84	76 0	67 5	53 5	50 0	36 0	14 5	14 5	14 5
3	142	119	99	86	76 0	67 0	51 5	48 7	34 5	14 0	14 0	14 0
4	138	118	100	88	78 0	69 0	53 5	50 9	36 5	14 5	14 5	14 5
5	153	129	105	90	81 5	71 0	54 0	50 5	35 0	14 5	14 5	14 5
6	103	98	91	82	75 5	67 5	53 5	50 4	36 5	14 5	14 5	14 5
7	98	88	85	78	73 0	66 0	53 0	50 0	36 0	14 5	14 5	14 5
8	82	78	75	71	67 5	64 0	53 0	49 9	37 0	14 5	14 5	14 5
9	88	84	81	76	71 0	65 5	53 0	49 8	37 0	14 5	14 5	14 5
10	81	77	74	70	67 0	63 5	53 0	50 1	38 0	14 5	14 5	14 5
11	78	74	71	68	65 0	62 0	53 0	49 8	38 0	15 5	14 5	14 5
12	86	83	80	75	70 5	66 0	53 0	49 4	37 0	14 5	14 5	14 5
13	149	125	102	88	78 0	69 0	53 0	48 8	35 5	14 5	14 5	14 5
14	88	86	82	76	72 5	66 0	52 5	49 0	37 0	14 5	14 5	14 5
14-A	88	86	82	76	72 5	65 0	51 5	49 0	37 0	22 5	23 5	23 5
14-B	88	86	82	76	71 5	65 0	52 5	49 5	39 0	34 5	35 5	34 5
14-C	88	86	81	76	71 5	64 5	53 0	50 5	41 0	39 5	40 5	39 5
14-D	88	86	81	76	72 0	65 0	54 5	52 5	46 0	45 5	45 5	45 5
14-E	88	86	81	75	71 5	65 5	56 5	54 9	50 0	49 5	49 5	49 5
14-F	88	86	81	75	71 5	65 5	58 5	57 5	54 0	54 5	54 5	54 5
14-G	88	86	81	75	72 0	67 5	62 5	60 5	59 0	58 5	58 5	58 5
15	84	76	71	67	65 0	60 5	53 0	50 1	37 0	20 5	16 5	17 5
16	87	77	72	68	66 0	62 0	53 5	49 9	38 0	22 5	18 5	18 5
17	100	95	90	82	75 0	66 5	53 0	49 6	36 0	14 5	14 5	14 5
18	85	77	72	68	67 0	63 5	54 0	50 8	38 0	22 5	18 5	18 5
19	107	84	74	68	66 0	62 5	54 0	50 7	36 0	26 5	25 5	25 5

TABLE VIII. Critical-flow Data and Exit Parameters for Test Section C7

Run	H_0, Btu/lb$_m$	G_c, lb$_m$/sec-ft^2	Exit Parameters		G_c/G_{cHE}	Run	H_0, Btu/lb$_m$	G_c, lb$_m$/sec-ft^2	Exit Parameters		G_c/G_{cHE}
			P_e, psia	x_E					P_e, psia	x_E	
1	418.5	529	42.5	0.174	1.71	31	328.2	1013	54.2	0.072	2.02
2	364.2	618	42.0	0.122	1.78	32	326.5	881	47.2	0.078	2.04
3	324.6	689	37.7	0.088	2.03	33	469.6	542	46.3	0.216	1.74
4	280.5	806	36.3	0.030	1.96	34	285.3	1015	51.2	0.035	1.88
5	235.7	3917	37.3	0.0032	8.07	35	283.9	951	45.5	0.040	2.01
6	306.0	911	44.8	0.061	2.12	36	254.4	3672	49.4	0.0046	6.13
7	304.9	803	39.5	0.067	2.11	37	252.8	2524	48.3	0.0048	4.29
8	338.1	667	39.9	0.099	1.94	38	340.1	825	47.6	0.091	1.99
9	372.9	599	40.9	0.131	1.85	39	264.7	1130	50.0	0.015	1.95
10	370.1	512	35.3	0.136	1.80	40	297.3	989	49.9	0.046	1.99
11	265.6	821	38.8	0.031	1.92	41	266.7	1055	49.1	0.019	1.88
12	371.5	650	43.8	0.126	1.85	42	271.0	1034	50.0	0.022	1.84
12-A	371.2	625	43.6	0.127	1.79	43	272.6	1008	50.5	0.023	1.81
12-B	371.1	635	43.6	0.126	1.81	44	272.9	1011	50.0	0.024	1.81
12-C	370.4	625	43.5	0.126	1.78	45	279.9	985	50.6	0.030	1.82
12-D	370.1	625	43.4	0.126	1.78	46	305.7	966	50.5	0.055	1.97
12-E	369.6	620	43.8	0.125	1.76	47	310.1	959	50.3	0.059	1.98
12-F	369.1	625	44.6	0.124	1.74	48	292.3	955	49.7	0.043	1.90
12-G	368.7	620	45.8	0.123	1.69	49	255.5	2109	50.1	0.0053	3.46
13	295.6	795	39.5	0.059	2.03	50	423.9	710	55.5	0.164	1.75
14	265.2	872	39.8	0.030	1.99	51	369.8	953	61.7	0.104	1.81
15	269.8	829	39.4	0.035	1.93	52	329.4	1143	60.6	0.066	1.97
16	271.3	851	40.6	0.035	1.94	53	477.9	714	61.8	0.210	1.71
17	272.1	859	40.5	0.036	1.96	54	474.8	655	56.8	0.212	1.73
18	280.6	842	41.1	0.044	1.94	55	286.2	1171	59.5	0.027	1.77
19	303.7	783	40.0	0.066	2.00	56	282.2	1301	59.0	0.022	1.92
20	308.4	751	40.4	0.070	1.95	57	299.2	1130	60.9	0.037	1.75
21	291.6	810	40.5	0.054	1.99	58	268.7	2354	60.3	0.0063	3.10
22	254.4	936	39.9	0.019	2.03	59	272.2	1488	60.0	0.011	2.01
23	247.1	1213	39.9	0.011	2.52	60	273.8	1377	60.5	0.012	1.87
24	241.2	2203	40.1	0.0048	4.30	61	274.9	1245	59.9	0.014	1.77
25	242.2	2222	40.1	0.0058	4.36	62	280.5	1119	59.2	0.020	1.64
26	245.5	1454	39.8	0.0099	3.00	63	307.4	1096	60.3	0.046	1.75
27	237.6	6460	39.0	0.0020	12.63	64	311.4	1098	60.5	0.050	1.79
28	421.4	608	48.2	0.169	1.72	65	293.6	1094	59.9	0.033	1.70
29	368.4	793	54.0	0.112	1.77	66	271.8	1757	60.0	0.010	2.36
30	366.3	704	47.2	0.117	1.81	67	266.9	4896	61.0	0.0032	6.10

TABLE IX. Pressure Profiles (psia) for Test Section C7

Run	Position												
	U8	U7	U6	U5	U4	U3	U2	U1	Exit	D1	D2	D3	D4
1	114	95	78	67	59.5	53.0	45.0	42.5	42.5	37.0	29.0	20.0	10.0
2	109	91	76	64	57.0	50.5	44.0	41.5	42.0	37.0	29.5	20.0	12.5
3	95	80	67	58	50.5	45.0	40.0	37.5	37.7	35.0	29.0	20.0	13.5
4	75	67	59	53	47.0	43.0	39.0	36.5	36.3	34.5	29.5	21.0	14.5
5	76	57	47	44	42.5	41.0	39.0	37.5	37.3	37.0	37.0	35.5	32.0
6	98	85	75	65	59.0	51.0	47.5	45.0	44.8	42.5	34.0	25.5	14.5
7	91	78	66	58	52.0	46.5	42.0	39.5	39.5	37.5	31.0	23.0	14.0
8	101	84	71	61	53.5	48.0	42.0	39.5	39.9	36.0	29.5	20.0	13.0
9	106	88	72	62	56.0	49.5	43.0	40.5	40.9	36.0	29.0	19.0	12.0
10	93	77	63	54	49.0	43.0	37.0	35.5	35.3	31.5	25.0	16.0	12.5
11	63	59	57	52	48.5	44.0	40.0	38.5	38.8	36.0	30.0	22.0	14.5
12	117	98	79	67	59.5	53.0	45.5	44.0	43.8	40.5	31.0	22.0	11.0
12-A	116	97	78	66	59.0	52.5	45.5	43.5	43.6	40.0	31.0	22.0	14.5
12-B	116	98	78	66	59.5	52.5	45.0	43.5	43.6	40.0	31.0	22.5	20.0
12-C	116	97	78	66	59.0	52.0	45.0	43.5	43.5	40.0	31.0	26.0	26.5
12-D	116	97	78	66	59.0	52.5	45.0	43.5	43.4	40.0	34.0	32.0	33.5
12-E	116	97	78	66	59.0	52.5	45.0	43.5	43.8	41.5	37.0	38.0	38.5
12-F	115	97	78	66	59.0	53.0	46.0	44.5	44.6	44.0	41.0	42.0	41.5
12-G	115	97	78	66	59.0	53.0	47.0	45.5	45.8	43.5	43.0	44.0	43.5
13	85	78	65	57	51.5	45.5	41.0	39.5	39.5	37.5	30.0	21.5	13.5
14	64	60	58	52	49.0	44.5	40.5	39.5	39.8	37.5	31.0	22.5	13.5
15	68	64	59	54	49.0	44.5	40.5	39.5	39.4	37.0	30.5	21.5	15.5
16	73	68	62	56	50.5	45.5	41.0	40.5	40.6	37.5	31.0	22.0	15.5
17	73	68	62	56	51.0	46.5	41.5	40.5	40.5	38.5	31.0	22.5	15.5
18	79	72	64	57	51.5	46.5	41.5	41.0	41.1	38.5	31.0	22.5	16.0
19	92	79	67	58	52.0	45.5	40.5	40.0	40.0	37.5	30.0	20.5	15.5
20	95	80	69	60	52.0	45.5	41.0	40.0	40.4	37.5	30.0	20.5	15.5
21	86	75	66	58	51.0	45.5	40.5	40.0	40.5	37.0	30.0	21.0	15.5
22	57	55	52	49	46.5	44.0	41.0	39.5	39.9	37.0	32.5	24.5	16.5
23	56	53	50	47	45.0	43.0	41.0	39.5	39.9	38.5	35.5	29.0	18.5
24	61	54	49	46	45.0	43.0	41.0	40.5	40.1	40.0	39.0	36.0	28.5
25	59	52	48	46	45.0	42.5	41.5	40.5	40.1	40.5	39.5	37.5	29.5
26	53	50	48	46	44.0	42.0	40.5	40.5	39.8	39.5	38.0	33.5	20.5
27	146	89	60	50	46.0	42.0	39.5	39.0	39.0	38.0	38.0	36.0	35.0
28	127	107	87	75	67.0	59.0	51.0	48.0	48.2	42.0	32.5	23.0	10.0
29	135	114	94	81	71.0	63.5	56.0	54.0	54.0	48.0	38.5	27.5	14.0
30	120	102	83	71	63.0	55.5	49.0	47.0	47.2	41.5	33.5	24.0	13.0
31	124	108	92	80	70.0	63.0	57.0	54.0	54.2	50.5	42.0	30.0	16.5
32	113	97	81	71	61.5	55.0	50.0	47.0	47.2	44.0	36.0	26.5	14.5
33	131	108	74	74	66.5	58.5	48.5	46.5	46.3	40.0	31.0	21.0	10.5
34	85	80	75	68	63.0	57.5	52.5	51.0	51.2	47.0	40.0	29.5	15.5
35	81	76	69	63	56.5	51.5	46.5	45.5	45.5	42.0	35.5	26.5	15.5
36	86	68	59	56	54.5	53.5	51.0	49.5	49.4	48.5	48.5	46.0	40.0
37	72	63	58	55	53.5	52.0	49.5	48.0	48.3	47.5	45.5	43.5	33.0
38	118	101	84	72	63.0	56.5	50.0	47.5	47.6	44.0	35.5	25.5	14.0
39	66	62	60	59	56.0	54.0	51.0	50.0	50.0	48.5	42.0	32.0	16.5
40	94	87	78	69	63.5	57.5	52.0	50.0	49.9	46.5	38.0	28.5	14.4
41	67	65	62	60	57.5	53.5	50.5	49.0	49.1	46.5	40.0	29.0	14.5
42	72	70	66	63	59.5	56.0	51.0	50.0	50.0	47.0	39.5	29.0	16.5
43	77	74	71	66	61.0	56.0	50.5	50.5	50.5	47.5	39.5	28.5	16.5
44	77	74	70	65	60.0	55.5	50.5	50.0	50.0	46.0	38.5	28.5	16.5
45	84	80	74	66	62.0	56.5	51.0	50.5	50.6	46.5	39.0	29.5	16.5
46	104	93	81	71	64.0	58.0	52.0	50.5	50.5	47.0	38.5	28.0	16.5
47	109	96	84	73	64.0	57.0	51.5	50.0	50.3	47.0	38.0	27.5	16.5
48	92	85	77	68	62.0	56.0	51.0	49.5	49.7	46.0	37.5	27.5	16.5
49	69	63	59	56	54.5	53.0	51.0	50.0	50.1	49.0	47.0	44.5	30.0
50	146	124	99	86	76.0	67.5	58.0	55.5	55.5	48.5	37.5	26.0	11.5
51	153	130	107	93	82.0	73.5	64.5	62.0	61.7	56.0	44.5	32.5	15.5
52	134	119	103	90	80.0	71.5	63.5	61.0	60.6	57.5	47.0	34.0	17.5
53	169	140	112	97	87.0	66.0	64.5	62.0	61.8	53.0	40.5	28.0	13.0
54	155	129	104	89	79.5	70.5	58.0	57.0	56.8	49.0	37.0	26.0	11.5
55	88	83	81	76	71.0	66.5	61.0	60.0	59.5	54.5	47.0	34.5	17.5
56	87	82	77	73	69.0	65.0	60.5	58.5	59.0	55.5	48.0	36.0	19.5
57	100	96	89	81	75.0	68.5	62.5	61.0	60.9	57.0	47.0	35.0	16.0
58	82	74	70	68	67.0	65.0	62.0	60.0	60.3	58.0	55.5	53.5	33.5
59	78	74	71	69	66.5	64.0	61.0	60.0	60.0	56.5	54.5	43.0	22.5
60	80	77	75	72	69.0	65.5	61.5	60.5	60.5	58.5	49.5	37.0	19.5
61	80	77	75	71	68.5	65.0	61.0	60.0	59.9	56.5	48.5	36.5	19.5
62	87	84	80	75	71.0	65.5	60.0	59.0	59.2	55.0	44.5	33.0	18.0
63	112	104	93	82	75.0	68.5	61.0	60.0	60.3	56.0	44.0	33.0	18.0
64	116	106	95	84	75.0	69.0	62.0	60.5	60.5	56.0	45.0	33.5	18.0
65	97	93	87	81	74.0	68.0	62.0	59.5	59.9	56.0	45.0	33.0	17.5
66	77	73	70	68	66.5	63.0	60.5	60.0	60.0	58.5	55.5	48.5	26.5
67	127	94	79	73	70.0	66.5	62.5	61.0	61.0	59.5	58.5	55.5	49.5

TABLE X. Critical-flow Data and Exit Parameters for Test Section R7

Run	H_0, Btu/lb$_m$	G_c, lb$_m$/sec-ft^2	Exit Parameters					G_c/G_{cHE}
			P_e, psia	x_E	α_e	$u_{\ell c}$, ft/sec	k_E	
1	270.2	1004	49.6	0.021	0.78	77.3	3.0	1.82
2	264.5	1110	49.6	0.016	0.70	61.0	3.3	1.96
3	259.6	1348	49.7	0.010	0.57	54.2	3.9	2.32
4	256.6	1912	49.9	0.0068	0.37	52.4	5.8	3.24
5	255.4	2278	49.4	0.0061	0.28	54.7	7.9	3.83
6	257.5	1669	49.8	0.0079	0.38	46.5	6.4	2.84
7	260.9	1280	49.6	0.012	0.59	54.2	4.2	2.22
8	312.2	1998	102.0	0.013	0.58	85.0	2.4	1.94
9	342.8	2826	148.0	0.015	0.49	101.0	2.6	1.96
10	288.0	892	49.8	0.039	0.94	257	1.3	1.75
11	257.6	1498	49.3	0.0087	0.39	42.5	6.8	2.55
12	267.9	1040	49.6	0.019	0.77	78.3	2.9	1.87
13	307.0	2473	98.0	0.011	0.34	66.4	5.2	2.37
14	317.4	1620	100.0	0.021	0.72	104.0	2.0	1.64
15	311.1	2290	102.0	0.012	0.34	62.0	5.8	2.21
16	348.1	2351	149.0	0.020	0.64	119.0	1.9	1.67
17	277.2	931	49.3	0.029				1.74
18	260.5	1267	49.9	0.011				2.19
19	310.2	866	50.1	0.060				1.79
20	251.7	4836	48.9	0.0025				8.15
21	257.2	1608	49.7	0.0077				2.73
22	251.9	3459	49.3	0.0025				5.70
23	254.8	1912	49.6	0.0053				3.21
24	251.9	3959	49.8	0.0019				6.53
25	254.0	5177	50.5	0.0030				8.42
26	253.6	2387	50.3	0.0035				3.89
27	369.6	705	49.5	0.118				1.75
28	316.3	864	50.8	0.065				1.82
29	298.3	882	50.3	0.049				1.76
30	335.4	4787	145.0	0.0080				3.21
31	344.9	2631	149.0	0.016				1.84
32	362.0	2010	150.0	0.035				1.52
33	332.2	1510	100.5	0.036				1.64
34	308.0	2387	100.0	0.010				2.27
35	303.9	3423	101.5	0.0053				3.17

TABLE XI. Pressure Profiles (psia) with Void-fraction Traverses for Test Section R7

Run		Position												
		U8	U7	U6	U5	U4	U3	U2	U1	Exit	D1	D2	D3	D4
1	Pressure	76	70	66	63	60.5	58.5	56.0	51.0	49.6	37.5	28.5	Vac[a]	17.0
	Void fraction				0.55	0.56	0.58	0.66	0.75	0.78				
2	Pressure	70	65	62	60	58.0	56.5	54.5	51.0	49.6	39.5	30.5	Vac[a]	17.0
	Void fraction				0.41	0.45	0.49	0.56	0.67	0.70				
3	Pressure	71	64	60	58	56.0	55.5	54.0	50.5	49.7	43.5	36.5	15.5	18.0
	Void fraction				0.39	0.42	0.45	0.50	0.55	0.57				
4	Pressure	76	65	59	58	56.5	55.5	54.0	51.0	49.9	47.0	44.5	25.0	21.0
	Void fraction				0.15	0.17	0.22	0.25	0.35	0.37				
5	Pressure	82	67	59	58	56.0	54.5	53.5	51.0	49.4	47.5	45.5	28.5	23.5
	Void fraction				0.12	0.12	0.14	0.17	0.23	0.28				
6	Pressure	71	62	58	57	55.5	54.5	53.5	50.5	49.8	46.0	42.5	21.0	19.0
	Void fraction				0.07	0.11	0.20	0.24	0.33	0.38				
7	Pressure	70	63	59	58	56.5	55.0	54.0	51.0	49.6	43.0	35.0	15.0	18.0
	Void fraction				0.36	0.39	0.41	0.52	0.56	0.59				
8	Pressure	150	135	125	120	116	115	111.0	103.5	102.0	84.5	67.0	28.5	23.5
	Void fraction				0.47	0.49	0.49	0.52	0.55	0.58	0.88			
9	Pressure	217	194	178	175	171	168	162	149	148	-	105	44.5	34.5
	Void fraction				0.14	0.19	0.24	0.31	0.43	0.49				

[a]Vac denotes pressure less than atmospheric.

TABLE XII. Pressure Profiles (psia) without Void-fraction Traverses for Test Section R7

Run	Position												
	U8	U7	U6	U5	U4	U3	U2	U1	Exit	D1	D2	D3	D4
10	89	83	77	70	66.5	62.0	58.5	50.0	49.8	34.5	25.5	Vac[a]	16.5
11	69	61	57	56	55.0	54.0	53.0	50.0	49.3	45.0	40.0	18.5	18.5
12	73	68	64	62	59.5	58.0	56.0	51.0	49.6	38.5	30.5	14.5	17.0
13	141	125	115	114	111	110	106.0	99.0	98.0	89.0	80.0	35.0	30.0
14	140	132	126	122	119	117	113	103.0	100.0	73.5	54.5	23.5	20.5
15	145	129	120	118	115	114	110.5	103.5	102.0	91.0	78.0	34.5	27.5
16	222	203	187	180	176	172	167	154	149.0	-[b]	86.0	36.0	29.0
17	79	74	70	66	63.0	60.5	57.0	51.0	49.3	35.0	26.5	Vac	16.5
18	69	63	60	59	57.0	55.5	54.0	51.0	49.9	42.5	34.0	15.5	17.5
19	112	105	84	74	69.0	65.5	61.5	52.5	50.1	34.5	26.0	Vac	16.0
20	173	109	69	65	61.0	57.5	54.5	51.5	48.9	47.5	47.0	41.5	38.0
21	70	62	58	57	56.0	54.5	53.5	51.0	49.7	45.5	41.5	20.5	19.5
22	117	83	63	62	59.0	57.0	55.0	51.0	49.3	47.5	46.5	38.0	31.5
23	83	70	61	59	57.0	55.0	53.5	50.5	49.6	45.5	42.0	23.0	20.0
24	136	92	68	66	61.5	59.0	56.0	52.0	49.8	47.5	47.5	39.0	34.0
25	194	120	73	69	63.0	59.0	55.5	53.0	50.5	48.5	48.5	42.5	39.5
26	94	78	65	62	59.5	57.5	55.5	51.5	50.3	47.0	44.5	29.0	23.5
27	143	117	91	79	73.0	68.5	63.5	52.5	49.5	32.5	22.5	Vac	14.5
28	118	106	87	76	71.0	66.5	62.5	53.0	50.8	35.0	26.0	Vac	16.0
29	100	94	81	72	68.0	64.0	60.5	52.5	50.3	35.5	26.5	Vac	16.5
30	286	219	178	174	168	164	160	150	145.0	-	-	78.5	58.0
31	228	204	185	178	174	169	165	153	149.0	-	97.0	41.5	32.5
32	229	219	205	196	192	186	178	157	150.0	102.0	73.0	30.0	24.5
33	163	155	144	136	131	127	119.0	105.5	101.5	69.5	51.5	21.5	19.5
34	165	143	127	121	117	115	109.0	103.0	100.0	87.5	74.5	34.0	27.5
35	194	158	132	127	122	118	113.0	104.0	100.5	92.0	84.0	48.5	37.5

[a]Vac denotes pressure less than atmospheric.
[b]- denotes pressure greater than range or gauge.

ACKNOWLEDGMENTS

I wish to express my gratitude to my coadvisors, Dr. Hans K. Fauske, who introduced me to the two-phase critical-flow problem and closely supervised the study; and Dr. Stuart T. McComas, who gave freely of his time and knowledge. Personal thanks are extended to Elmer Gunchin and Leonard Indykiewicz, who aided in the construction, maintenance, and operation of the experimental apparatus, and to Matthew Gats for his technical assistance.

This research was supported by a fellowship from the Associated Midwest Universities and carried out under the auspices of the United States Atomic Energy Commission, Division of Reactor Development, Engineering Development Branch. The investigation was conducted at Argonne National Laboratory, Reactor Engineering Division.

REFERENCES

1. Andeen, G. B., and P. Griffith, *The Momentum Flux in Two-phase Flow*, MIT Dept. Mech. Eng. Report 4547-38 (1965).
2. Christensen, H., *Power-to-Void Transfer Functions*, ANL-6385 (July 1961).
3. Collingham, R. E., and J. C. Firey, *Velocity of Sound Measurements in Wet Steam*, I. & E. C. Process Design and Dev *2*, 197 (1963).
4. Cruver, J. E., *Metastable Critical Flow of Steam-Water Mixtures*, Ph.D. thesis, University of Washington (1963).
5. Cruver, J. E., and R. W. Moulton, *Critical Flow of Liquid Vapor Mixtures*, AIChE J *13*, 52 (1967).
6. Cruver, J. E., and R. W. Moulton, *Metastable Critical Flow of Steam-Water Mixtures*, Presented at Fund. of Fluid Mech. Sym., AIChE Meeting, Detroit (1966).
7. England, W. G., J. C. Firey, and O. E. Trapp, *Additional Velocity of Sound Measurements in Wet Steam*, I. & E. C. Process Design and Dev. *5*, 198 (1966).
8. Faletti, D. W., and R. W. Moulton, *Two-phase Critical Flow of Steam-Water Mixtures*, AIChE J *9*, 247 (1963).
9. Fauske, H. K., *Contribution to the Theory of Two-phase, One-component Critical Flow*, ANL-6633 (Oct 1962).
10. Fauske, H. K., *A Theory for Predicting Pressure Gradients for Two-phase Critical Flow*, Nucl. Sci. Eng. *17*, 1 (1963).
11. Fauske, H. K., *Two-phase Critical Flow with Applications to Liquid-Metal Systems (Mercury, Cesium, Rubidium, Potassium, Sodium, and Lithium)*, ANL-6779 (Oct 1963).
12. Fauske, H. K., and T. C. Min, *A Study of the Flow of Saturated Freon-11 through Apertures and Short Tubes*, ANL-6667 (Jan 1963).
13. Fauske, H. K., *The Discharge of Saturated Water through Tubes*, Chem. Eng. Prog. Sym. Ser. *61*, 210 (1965).
14. Fauske, H. K., *Two-phase Two- and -One Component Critical Flow*, Proc. of Sym. on Two-phase Flow, University of Exeter, Devon, England, *3*, SG101 (1965).
15. Giffen, E., and T. F. Crang, *Steam Flow in Nozzles; Velocity Coefficients at Low Steam Speeds*, Proc. Inst. Mech. Engrs. (London) *155*, 83 (1946).
16. Gouse, S. W., Jr., *An Index to Two-phase Gas-Liquid Flow Literature - Part I*, MIT Dept. of Mech. Eng. Report DSR-8734-1 (1963).
17. Gouse, S. W., Jr., *An Index to Two-phase Gas-Liquid Flow Literature - Part II*, MIT Dept. of Mech. Eng. Report DSR 8734-4 (1964).
18. Gouse, S. W., Jr., and G. A. Brown, *A Survey of the Velocity of Sound in Two-phase Mixtures*, ASME Preprint No. 64-WA/FE-35 (1964).
19. Gouse, S. W., Jr., "Void Fraction Measurements," *Two-phase Gas-Liquid Flow*, Notes from MIT Summer Program (1964).

20. Hooker, H. H., and G. F. Popper, *A Gamma-ray Attenuation Method for Void Fraction Determinations in Experimental Boiling Heat Transfer Test Facilities*, ANL-5766 (Nov 1958).

21. Isbin, H. S., J. E. Moy, and A. J. R. Cruz, *Two-phase Steam-Water Critical Flow*, AIChE J *3*, 361 (1957).

22. Isbin, H. S., H. K. Fauske, T. Grace, and I. Garcia, *Two-phase Steam-Water Pressure Drops for Critical Flow*, Mech. Engr. (London) (1962).

23. James, R., *Steam-Water Critical Flow through Pipes*, Proc. Inst. Mech. Engrs. (London) *176*, 741 (1962).

24. Jones, J. B., and G. A. Hawkins, *Engineering Thermodynamics*, John Wiley & Sons, Inc. (1960).

25. Karplus, H. B., *The Velocity of Sound in a Liquid Containing Gas Bubbles*, COO-248 (1958).

26. Karplus, H. B., *Propagation of Pressure Waves in a Mixture of Water and Steam*, ARF-4132-12 (1961).

27. Keenan, J. H., and F. G. Keyes, *Thermodynamic Properties of Steam*, John Wiley & Sons, New York (1936).

28. Kepple, R. R., and T. V. Tung, *Two-phase (Gas-Liquid) System: Heat Transfer and Hydraulics, and Annotated Bibliography*, ANL-6734 (July 1963).

29. Klingebiel, W. J., *Critical Flow Slip Ratios of Steam-Water Mixtures*, Ph.D. thesis, University of Washington (1964).

30. Levy, S., *Steam Slip-Theoretical Prediction from Momentum Model*, Trans. ASME J Heat Transfer *82-C*, 113 (1960).

31. Levy, S., *Prediction of Two-phase Critical Flow Rate*, Trans. ASME J Heat Transfer *87-C*, 53 (1965).

32. Linning, D. L., *The Adiabatic Flow of Evaporating Fluids in Pipes of Uniform Bore*, Proc. Inst. Mech. Engrs. (London) *1B*, No. 2, 64 (1952).

33. Martinelli, R. C., and D. B. Nelson, *Prediction of Pressure Drop during Forced Circulation Boiling of Water*, Trans. ASME *70*, 695 (1948).

34. Massena, W. A., *Steam-Water Pressure Drop and Critical Discharge Flow, A. Digital Computer Program*, HW-65706 (1960).

35. Moody, F. J., *Maximum Flow Rate of a Single Component, Two-phase Mixture*, Trans. ASME J Heat Transfer *87-C*, 134 (1965).

36. Muir, J. F., and R. Eichhorn, *Compressible Flow of an Air-Water Mixture through a Vertical, Two-dimensional, Converging-Diverging Nozzle*, Proc. 1963 Heat Transfer and Fluid Mech. Inst., 183 (1963).

37. Nahavandi, A. N., and M. P. Rashevsky, *A Digital Computer Program for Critical Flow Discharge of Two-phase Steam-Water Mixtures*, Carolinas Virginia Nuclear Power Associates, Inc., CVNA-128 (1962).

38. Nahavandi, A. N., and R. F. Von Hollen, *Two-phase Pressure Gradients in the Approach Region to Critical Flow*, Nucl. Sci. Eng. *22*, 463 (1965).

39. Petrick, M., and B. S. Swanson, *A Radiation Attentuation Method of Measuring Density of Two-phase Fluids*, Rev. Sci. Instr. *29*, 1079 (1958).

40. Rose, S. C., and P. Griffith, *Flow Properties of Bubbly Mixtures*, ASME Preprint 65-HT-58 (1965).

41. Smith, R. V., *Choking Two-phase Flow Literature Summary and Idealized Solutions for H_2, N_2, O_2 and Refrigerants 11 and 12*, NBS-TN-179 (1963).

42. Shapiro, A. H., *The Dynamics and Thermodynamics of Compressible Fluid Flow*, The Ronald Press (1953).

43. Stodola, A., *Steam and Gas Turbines*, McGraw-Hill (1927).

44. Semenov, N. I., and S. I. Kosterin, *Results of Studying the Speed of Sound in Moving Gas-Liquid Systems*, Thermal Engineering *6*, 59 (1964).

45. Starkman, E. S., V. E. Schrock, K. F. Neusen, and D. J. Maneely, *Expansion of a Very Low Quality Two-phase Fluid through a Convergent-Divergent Nozzle*, Trans. ASME J Basic Engr. *86-D*, 247 (1964).

46. Uchida, H., and H. Nariai, *Discharge of Saturated Water through Pipes and Orifices*, Proc. of the Third Inter. Heat Transfer Con. *5*, 1 (1966).

47. Vance, W. H., *Study of Slip Ratios for the Flow of Steam-Water Mixtures at High Void Fractions*, Ph.D. thesis, University of Washington (1962).

48. Vogrin, J. A., Jr., *An Experimental Investigation of Two-phase, Two-component Flow in a Horizontal, Converging-Diverging Nozzle*, ANL-6754 (July 1963).

49. Zaloudek, F. R., *The Low Pressure Critical Discharge of Steam-Water Mixtures from Pipes*, HW-68936 (1961).

50. Zaloudek, F. R., *The Critical Flow of Hot Water through Short Tubes*, HW-77594 (1963).

51. Zaloudek, F. R., *The Low Pressure Critical Discharge of Steam-Water Mixtures from Pipe Elbows and Tees*, BNWL-34 (1965).

52. Zivi, S. M., *Estimation of Steady-state Void Fraction by Means of the Principle of Minimum Entropy Production*, Trans. ASME J Heat Transfer *86-C*, 247 (1964).

53. *Radiological Health Handbook*, Health, Education, and Welfare Dept. Doc., PR 121784R (1960).